# CREDAL WRAPPER OF MODEL AVERAGING FOR UNCERTAINTY ESTIMATION IN CLASSIFICATION

**Anonymous authors**
Paper under double-blind review

## ABSTRACT

This paper presents an innovative approach, called *credal wrapper*, to formulating a credal set representation of model averaging for Bayesian neural networks (BNNs) and deep ensembles (DEs), capable of improving uncertainty estimation in classification tasks. Given a finite collection of single predictive distributions derived from BNNs or DEs, the proposed credal wrapper approach extracts an upper and a lower probability bound per class, acknowledging the epistemic uncertainty due to the availability of a limited amount of distributions. Such probability intervals over classes can be mapped on a convex set of probabilities (a credal set) from which, in turn, a unique prediction can be obtained using a transformation called *intersection probability transformation*. In this article, we conduct extensive experiments on several out-of-distribution (OOD) detection benchmarks, encompassing various dataset pairs (CIFAR10/100 vs SVHN/Tiny-ImageNet, CIFAR10 vs CIFAR10-C, CIFAR100 vs CIFAR100-C and ImageNet vs ImageNet-O) and using different network architectures (such as VGG16, ResNet-18/50, EfficientNet B2, and ViT Base). Compared to the BNN and DE baselines, the proposed credal wrapper method exhibits superior performance in uncertainty estimation and achieves a lower expected calibration error on corrupted data.

## 1 INTRODUCTION

Despite their success in various scientific and industrial areas, deep neural networks often generate inaccurate and overconfident predictions when faced with uncertainties induced by, e.g. out-of-distribution (OOD) samples, natural fluctuations, or adversarial disruptions (Papernot et al., 2016; Zhang et al., 2021; Hüllermeier & Waegeman, 2021; Hendrycks & Gimpel, 2016). Properly estimating the uncertainty associated with their predictions is key to improving the reliability and robustness of neural networks (Senge et al., 2014; Kendall & Gal, 2017; Sale et al., 2023b). Researchers commonly distinguish two types of uncertainty in neural networks (and machine learning models in general). Aleatoric uncertainty (AU), also known as data uncertainty, arises from inherent randomness such as data noise, and is irreducible. Epistemic uncertainty (EU) stems from the lack of knowledge of the data generation process and can be reduced with increased availability of training data (Hüllermeier & Waegeman, 2021). The distinction between AU and EU can be beneficial in applications such as active learning or OOD detection, particularly in safety-critical and practical fields such as autonomous driving (Zhou et al., 2012) and medical diagnosis (Lambrou et al., 2010). For example, in active learning, the objective is to avoid inputs that exhibit high AU but low EU. Similarly, effective EU estimation can prevent the misclassification of ambiguous in-distribution (ID) examples as OOD instances (Mukhoti et al., 2023), for the inherent ambiguity of the former does not arise from more epistemically uncertain regions of the ID distribution.

To represent and estimate both AU and EU, researchers have recently proposed neural networks able to output a 'second-order' representation in the target space, to express their uncertainty about a prediction's uncertainty itself (Hüllermeier et al., 2022; Sale et al., 2023b; Cuzzolin, 2024). Sampling-based approaches, among which Bayesian neural networks (BNNs) and deep ensembles (DEs), have emerged as powerful methods in this domain.

The BNN framework (Blundell et al., 2015; Gal & Ghahramani, 2016; Krueger et al., 2017; Mobiny et al., 2021), in particular, quantifies uncertainty by learning a posterior distribution over a network's weights; this, in turn, is used to predict a 'second-order' distribution (i.e., a distribution of

distributions (Hüllermeier & Waegeman, 2021)) over the target space. While BNNs are straightforward to construct, their training presents a significant challenge due to inherent computational complexity. Consequently, several approximation algorithms have been developed, such as sampling methods (Neal et al., 2011; Hoffman et al., 2014; Hobbhahn et al., 2022; Daxberger et al., 2021; Tran et al., 2020; Rudner et al., 2022), variational inference approaches (Blundell et al., 2015; Gal & Ghahramani, 2016), and Laplace approximation methodologies (Jospin et al., 2022). As computing the exact 'second-order' distribution generated by full Bayesian inference at prediction time is of prohibitive complexity, Bayesian model averaging (BMA) is often applied in practice (Gal & Ghahramani, 2016). The latter entails sampling a finite set of deterministic weight values from the posterior (obtained after training) to generate a collection of single (softmax) distributions. However, in practice, BNNs are generally challenging to scale to large datasets and architectures due to the high computational complexity (Mukhoti et al., 2023), and a limited number of samples is often used for BMA to reduce the inference complexity.

DEs (Lakshminarayanan et al., 2017), an established alternative approach for quantifying uncertainty, have been recently serving as a strong baseline in deep learning (Ovadia et al., 2019; Gustafsson et al., 2020; Abe et al., 2022; Mucsányi et al., 2024). DEs marginalize multiple standard neural network models to obtain a predictive distribution instead of explicitly inferring a distribution over parameters such as BNNs (Lakshminarayanan et al., 2017; Band et al., 2021). At prediction time, DEs average a finite set of single probability distributions for classification. Despite their successes in uncertainty quantification, a recent study has shown that DEs may demonstrate relatively low quality of EU estimation (Abe et al., 2022). They have also been criticized because of their substantial demand for memory and computational resources (Liu et al., 2020; He et al., 2020).

As previously discussed, a practical challenge in both BNNs and DEs at prediction time is the limited number of individual distributions (e.g., most papers use up to five) used to approximate the true predictive distribution and quantify uncertainty. Therefore, an intriguing research question arises here: *Can the uncertainty quantification performance of the sampling-based approaches be enhanced given the constrained number of predictive distributions?*

**Novelty and Contribution** In response, this paper presents an innovative method for formulating a credal set representation for both BNNs with BMA and DEs, capable of improving their uncertainty estimation in classification tasks, which we term *credal wrapper*. Given a limited collection of single distributions derived, at prediction time, from either BNNs or DEs, the proposed approach computes a lower and an upper probability bound per class, i.e., a collection of probability intervals (Tessem, 1992; De Campos et al., 1994), to acknowledge the epistemic uncertainty about the sought exact predictive distribution induced by the limited information actually available.

Such lower and upper bounds on each class' probability induce, in turn, a convex set of probabilities, known as *credal set* (Levi, 1980; De Campos et al., 1994). From such a credal set (the output of our credal wrapper), an *intersection probability* can be derived, in whose favor theoretical arguments exist as the natural way of mapping a credal set to a single probability (Cuzzolin, 2009; 2022).

Extensive experiments are performed on several OOD detection benchmarks including different dataset pairs (CIFAR10/100 vs SVHN/Tiny-ImageNet, CIFAR10 vs CIFAR10-C, CIFAR100 vs CIFAR100-C, and ImageNet vs ImageNet-O) and utilizing various network architectures (VGG16, ResNet-18/50, EfficientNet B2 and ViT Base). Compared to the BNN and DE baselines, the proposed *credal wrapper* demonstrates improved uncertainty estimation and a lower expected calibration error on the corrupted test instances when using the intersection probability for class prediction.

**Other Related Work** Numerous mathematical theories, such as subjective probability (De Finetti, 2017), possibility theory (Zadeh, 1978; Dubois & Prade, 1990), credal sets (Kyburg Jr, 1987; Levi, 1980), probability intervals, random sets (Nguyen, 1978), and imprecise probability theory (Walley, 1991), have been devised to estimate the (epistemic) uncertainty in response to the challenge posed by the limited availability of information (in our case, a limited number of sampled single distributions). These theories state that the exact probability distribution is inaccessible and that the available evidence should instead be used to impose specific constraints on the unknown distribution.

Among them, probability intervals represent one of the simplest approaches and have attracted significant interest among researchers (Yager & Kreinovich, 1999; Guo & Tanaka, 2010; Wei et al., 2021; Cuzzolin, 2022). Instead of providing point-valued probabilities, probability intervals assume that the probability values $p(y)$ of the elements (e.g., classes) of the target space (e.g., the set of

classes) belong to an interval $p_L(y) \leq p(y) \leq p_U(y)$, delimited by a lower probability bound $p_L(y)$ and an upper probability bound $p_U(y)$. Researchers have claimed that probability intervals may express uncertainty more appropriately than single probabilities (De Campos et al., 1994; Cano & Moral, 2002; Guo & Tanaka, 2010), particularly in situations where: (i) limited information is available to estimate unknown and exact probabilities; (ii) individual pieces of information are in conflict: e.g., when three predictors for the weather condition (rainy, sunny, or cloudy) predict probability vectors $(0.2, 0.6, 0.2)$, (0.1, 0.2, 0.7), and (0.7, 0.1, 0.2), respectively. Such undesirable scenarios can arise when BNNs or DEs use a limited number of predictive samples, as we discuss here.

Credal sets have recently attracted increasing attention within the broader field of machine learning for uncertainty quantification (Zaffalon, 2002; Corani & Zaffalon, 2008; Corani et al., 2012; Mauá et al., 2017; Hüllermeier & Waegeman, 2021; Shaker & Hüllermeier, 2021; Sale et al., 2023a). The advantage of adopting credal sets is the integration of notions of the set and probability distribution in a single and unified framework. Using credal sets, rather than individual distributions, arguably allows models to more naturally express epistemic uncertainty (Corani et al., 2012; Hüllermeier & Waegeman, 2021). Concerning deep neural networks, 'imprecise' BNNs (Caprio et al., 2024) modeling the network weights and predictions as credal sets have been proposed. Despite demonstrating robustness, the computational complexity of imprecise BNNs is comparable to that of the ensemble of BNNs, posing significant challenges for their widespread application.

In addition to BNNs and DEs, evidential deep learning models (Malinin & Gales, 2018; 2019; Malinin et al., 2019; Charpentier et al., 2020) have also been developed that generate a Dirichlet distribution (another type of 'second-order' representation) in the target space. A drawback of these methods is the fact that suitable Dirichlet distribution labels are not available at training time. Further, the behaviour of these models often deviates from theoretical EU assumptions (Ulmer et al., 2023). Recent research (Juergens et al., 2024) has shown that evidential methods often fail to faithfully represent EU, and that the resulting EU measures lack a meaningful quantitative interpretation.

**Paper Outline** The rest of the paper is structured as follows. Sec. 2 presents how uncertainty estimation works in different model classes. Sec. 3 introduces our credal wrapper in full detail. Sec. 4 describes the experimental validations. Sec. 5 summarizes our conclusion and future work. Appendices report additional experiments in §A and implementation details in §B, respectively.

## 2 Uncertainty Estimation in Different Model Classes

**Bayesian Neural Networks** BNNs model network parameters, i.e., weights and biases, as probability distributions. The resulting predictive distributions can thus be seen as 'second-order' distributions, i.e., probability distributions of distributions (Hüllermeier & Waegeman, 2021). As mentioned, for computational reasons, BMA is often applied for BNN inference (Gal & Ghahramani, 2016). Namely, in a classification context, we obtain

$$\tilde{\boldsymbol{p}} = \frac{1}{N_p} \sum_{i=1}^{N_p} \boldsymbol{p}_i = \frac{1}{N_p} \sum_{i=1}^{N_p} h_{\text{bnn}}^{\boldsymbol{\omega}_i}(\boldsymbol{x}), \tag{1}$$

where $\boldsymbol{p}_i$ is the sampled prediction from the deterministic model ($h_{\text{bnn}}^{\boldsymbol{\omega}_i}$) parametrized by $\boldsymbol{\omega}_i$, $N_p$ is the number of samples, and $\tilde{\boldsymbol{p}}$ is the averaged probability. The parameter vector $\boldsymbol{\omega}_i$ is obtained from the $i$-th sampling instance of the parameter posterior distribution of BNNs (Jospin et al., 2022).

Employing Shannon entropy as the uncertainty measure, the total uncertainty (TU) and AU in BNNs can be approximately quantified by calculating the entropy of the averaged prediction and averaging the entropy of each sampled prediction (Hüllermeier & Waegeman, 2021), respectively, as follows:

$$\text{TU} := H(\tilde{\boldsymbol{p}}) = -\sum_k^C \tilde{q}_k \log_2 \tilde{q}_k, \ \text{AU} := \tilde{H}(\boldsymbol{p}) = \frac{1}{N_p} \sum_{i=1}^{N_p} H(\boldsymbol{p}_i) = -\frac{1}{N_p} \sum_{i=1}^{N_p} \sum_k^C p_{i_k} \log_2 p_{i_k}, \tag{2}$$

where $\tilde{q}_k$ and $p_{i_k}$ are the $k$-th elements of the probability vectors $\tilde{\boldsymbol{p}}$ and $\boldsymbol{p}_i$ across the $C$ classes, respectively. An estimate of epistemic uncertainty can then be derived as EU $:= H(\tilde{\boldsymbol{p}}) - \tilde{H}(\boldsymbol{p})$ (Depeweg et al., 2018), which can be interpreted as an approximation of 'mutual information' (Hüllermeier et al., 2022; Hüllermeier & Waegeman, 2021).

**Deep Ensembles** DEs generate an averaged prediction from a set of $M$ individually-trained standard neural networks (SNNs), as follows:

$$\tilde{\boldsymbol{p}} = \frac{1}{M} \sum_{m=1}^{M} h_m(\boldsymbol{x}) = \frac{1}{M} \sum_m^M \boldsymbol{p}_m, \tag{3}$$

where $\boldsymbol{p}_m$ denotes the single probability vector provided by the $m$-th SNN. Considered by some to be an approximation of BMA (Wilson & Izmailov, 2020; Abe et al., 2022), DEs also quantify TU, AU, and EU as in eq. (2), where the sampled single probability vector $\boldsymbol{p}_i$ is replaced by $\boldsymbol{p}_m$.

**Credal Sets** Uncertainty quantification for credal sets is an active research subject (Hüllermeier & Waegeman, 2021; Sale et al., 2023a). To that extent, researchers have developed the concepts of generalized entropy (Abellán et al., 2006) and generalized Hartley (GH) measure (Abellán & Moral, 2000; Hüllermeier et al., 2022). However, applying the GH measure in practice is challenging due to the high computational cost of solving constrained optimization problems involving $2^C$ subsets (Hüllermeier & Waegeman, 2021; Hüllermeier et al., 2022), particularly when the number of classes $C$ is large (e.g., $C = 100$). The width of the probability interval has also been proposed as an EU measure (Hüllermeier et al., 2022), but is only applicable to binary cases. As a result, we opt for generalized entropy. Given a credal set prediction, denoted by $\mathbb{P}$, its upper and lower entropy, $\overline{H}(\mathbb{P})$ and $\underline{H}(\mathbb{P})$, can be calculated as a generalization of the classical Shannon entropy, allowing us to estimate the TU and AU for a credal prediction (Abellán et al., 2006), as follows:

$$\text{TU} := \overline{H}(\mathbb{P}) = \max_{\boldsymbol{p} \in \mathbb{P}} H(\boldsymbol{p}), \quad \text{AU} := \underline{H}(\mathbb{P}) = \min_{\boldsymbol{p} \in \mathbb{P}} H(\boldsymbol{p}). \tag{4}$$

Such measures capture the maximal and the minimal Shannon entropy within the credal set, respectively. The level of EU can then be measured by their difference, namely $\text{EU} := \overline{H}(\mathbb{P}) - \underline{H}(\mathbb{P})$.

## 3 Methodology

Inspired by the use of probability intervals for decision-making (Yager & Kreinovich, 1999; Guo & Tanaka, 2010), we propose to build probability intervals by extracting the upper and lower bound per class from the given set of limited (categorical) probability distributions, validating this choice via extensive experiments in Section 4. E.g., consider again the task of predicting weather conditions (rainy, sunny, or cloudy). When receiving three probability values for the *rainy* condition, e.g., 0.2, 0.1, and 0.7, using probability intervals we model the uncertainty on the probability of the rainy condition as $[0.1, 0.7]$. Each probability interval system can determine a convex set of probabilities over the set of classes, i.e., a credal set. Such a credal set is a more natural model than individual distributions for representing the epistemic uncertainty encoded by the prediction, as it amounts to constraints on the unknown exact distribution (Hüllermeier & Waegeman, 2021; Shaker & Hüllermeier, 2021; Sale et al., 2023a). Nevertheless, a single predictive distribution, termed *intersection probability*, can still be derived from a credal set to generate a unique class prediction for classification purposes. Our credal wrapper framework is depicted in Figure 1. The remainder of this section discusses the credal wrapper generation, a method for computational complexity reduction for uncertainty estimation, and the intersection probability, in this order.

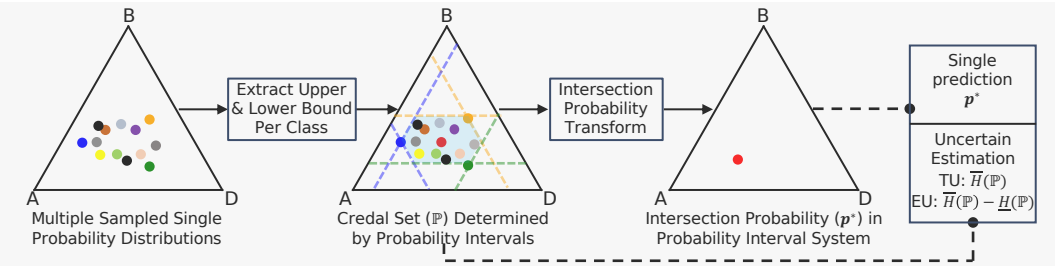


Figure 1: Credal wrapper framework for a three-class (A, B, D) classification task. Given a set of individual probability distributions (denoted as single dots) in the simplex (triangle) of probability distributions of the classes, probability intervals (parallel lines) are derived by extracting the upper and lower probability bounds per class, using eq. (5). Such lower and upper probability intervals induce a credal set on $\{\text{A, B, D}\}$ ($\mathbb{P}$, light blue convex hull in the triangle). A single intersection probability (the red dot) is computed from the credal set using the transform in eq. (5). Uncertainty is estimated in the mathematical framework of credal sets in eq. (4).

**Credal Wrapper Generation** Given a set of $N$ individual distributions from BNNs or DEs, an upper and a lower probability bound for $k$-th class element, denoted as $p_{U_k}$ and $p_{L_k}$, respectively, can be obtained from

$$p_{U_k} = \max_{n=1,..,N} p_{n,k}, \quad p_{L_k} = \min_{n=1,..,N} p_{n,k}, \tag{5}$$

where $p_{n,k}$ denotes the $k$-th element of the $n$-th single probability vector $\boldsymbol{p}_n$. Such probability intervals over $C$ classes determine a non-empty credal set $\mathbb{P}$, as follows (Moral-García & Abellán, 2021; De Campos et al., 1994):

$$\mathbb{P}=\{\boldsymbol{p} \mid \boldsymbol{p} \in \Delta^{C-1} \text{ and } p_k \in [p_{L_k}, p_{U_k}]\ \forall k=1,2,...,C\} \text{ s.t. } \sum_k^C p_{L_k} \leq 1 \leq \sum_k^C p_{U_k}, \tag{6}$$

where $\boldsymbol{p}$ denotes the valid (normalized) probability vector and $\Delta^{C-1}$ represents the probability simplex on the set of $C$ classes. The condition in eq. (6) guarantees that individual probabilities in the credal set satisfy the normalization condition, and their probability value per class is constrained to the given probability interval. It can be readily proven that the probability intervals generated in eq. (5) meet the above condition, as follows:

$$\sum_k^C p_{L_k} = \sum_k^C \min_{n=1,..,N} p_{n,k} \leq \sum_k^C p_{n^*,k} = 1 \leq \sum_k^C \max_{n=1,..,N} p_{n,k} = \sum_k^C p_{U_k}, \tag{7}$$

where $n^*$ is any index in $1,\ldots,N$. Computing $\overline{H}(\mathbb{P})$ in eq. (4) for uncertainty estimation, on the other hand, requires solving the following optimization problems:

$$\overline{H}(\mathbb{P}) = \text{maximize} \sum_k^C -p_k \cdot \log_2 p_k \text{ s.t. } \sum_k^C p_k = 1 \text{ and } p_k \in [p_{L_k}, p_{U_k}]\ \forall k=1,...,C, \tag{8}$$

which can be addressed by using a standard solver, such as the SciPy optimization package (Virtanen et al., 2020). To calculate $\underline{H}(\mathbb{P})$ in eq. (4), $\text{maximize}$ is simply replaced by $\text{minimize}$. We further discuss an alternative approach for generating credal sets in Appendix §C.

**Computational Complexity Reduction Method** The convex optimization problem in eq. (8) may present a computational challenge for a large value of $C$ (e.g., $C = 1000$). To mitigate this issue, we propose an approach, termed *Probability Interval Approximation* (PIA), in Algorithm 1. The PIA method initially identifies the top $J-1$ relevant classes by sorting the probability values of the intersection probability $\boldsymbol{p}^*$ (detailed in eq. (9)) below) in descending order. Then, the remaining elements are merged into a single class whose upper and lower probability are computed. As a result, the dimension of the approximate probability interval is reduced from $C$ to $J$.

**Algorithm 1** Probability Interval Approximation

**Input:** $[p_{L_k}, p_{U_k}]$ for $k=1,..C$; Intersection probability $\boldsymbol{p}^*$; Chosen number of classes $J$
**Output:** Approximated probability intervals $[r_{L_j}, r_{U_j}]$ for $k=1,..J$

1: Compute the index vector for sorting $\boldsymbol{p}^*$ in descending order as $\boldsymbol{m} := (m_1, m_2, ..., m_C)$ for $p^*_{m_1} \geq p^*_{m_2} \geq ... \geq p^*_{m_C}$
2: Calculate the upper and lower probability per selected class as $r_{L_j} := p_{L_{m_j}}, r_{U_j} := p_{U_{m_j}}$ for $j=1,...,J-1$
3: Calculate upper and lower probability for deselected classes as $r_{L_J} = \max(1-\sum_{i=m_J}^{m_C} p_{U_i}, \sum_{j=1}^{J-1} r_{L_j})$; $r_{U_J} = \min(1-\sum_{i=m_J}^{m_C} p_{L_i}, \sum_{j=1}^{J-1} r_{U_j})$

**Intersection Probability** In classification tasks, it is desirable to eventually map a credal set to a single probability prediction to make a unique class prediction. In our credal wrapper, from the probability interval predictions defined in eq. (5), we derive a single *intersection probability* vector for class prediction (Cuzzolin, 2022) as the unique probability distribution which (i) ensures that the derived single probability is normalized within the probability interval system, and (ii) assumes equal trust in the probability intervals for each class, since there is no justification for treating them differently (Cuzzolin, 2022). Mathematically, the intersection probability, $\boldsymbol{p}^*$, must satisfy

$$p^*_k = p_{L_k} + \alpha \cdot (p_{U_k} - p_{L_k})\ \forall k=1,...,C \tag{9}$$

where $p^*_k$ is the $k$-th element of $\boldsymbol{p}^*$ under a constant $\alpha \in [0,1]$. This is a convex combination of $p_{L_k}$ and $p_{U_k}$, so that $p^*_k \in [p_{L_k}, p_{U_k}]$. Due to the normalization constraint, $\sum_k^C p^*_k = 1$, it follows that:

$$\sum_k^C \big(p_{L_k} + \alpha(p_{U_k} - p_{L_k})\big) = 1 \Rightarrow \sum_k^C (p_{L_k}) + \alpha \sum_k^C (p_{U_k} - p_{L_k}) = 1. \tag{10}$$

As a result, the unique $\alpha$ can be computed as follows (Cuzzolin, 2022):

$$\alpha = \big(1 - \sum_k^C p_{L_k}\big) / \big(\sum_k^C (p_{U_k} - p_{L_k})\big). \tag{11}$$

The intersection probability is thus given by eq. (9) with $\alpha$ as given in eq. (11). The intersection probability transform follows clear rationale principles and does not suffer from the drawbacks of

other potential transforms. Let us see this in detail. (i) Taking the average probability value of the original sampled distributions produces a valid probability vector that falls within the probability interval system. However, such a transform does not leverage the probability bounds, thus violating the semantics of probability intervals (Guo & Tanaka, 2010; Cano & Moral, 2002) (and also exhibiting inferior performance in the experiments). (ii) Selecting the midpoint of each probability interval $[p_L, p_U]$, instead, does not generally result in a valid normalized probability vector. (iii) Normalizing the lower or the upper probability vectors, i.e., taking $\hat{p}_{U_k} = p_{U_k} / \sum_k^C p_{U_k}$ or $\hat{p}_{L_k} = p_{L_k} / \sum_k^C p_{L_k}$, yields a probability that is not guaranteed to be consistent with the interval system (Cuzzolin, 2020). In Appendix §D, we further discuss the limit behavior of the intersection probability when the number of sampled probability distributions goes to infinity.

## 4 Experimental Validation

In this section, we apply OOD detection benchmarks for EU quantification assessment OOD (Mukhoti et al., 2023; Mucsányi et al., 2024). Regarding OOD detection, a model is expected to exhibit high EU estimates on OOD samples in comparison to in-domain (ID) instances. Consequently, superior OOD detection performance provides evidence of the enhanced uncertainty estimation quality. To assess OOD detection performance, we use the AUROC (Area Under the Receiver Operating Characteristic curve) and AUPRC (Area Under the Precision-Recall curve) scores. Greater scores indicate a higher quality of uncertainty estimation. In addition to OOD detection performance, expected calibration error (ECE) (Guo et al., 2017; Nixon et al., 2019) is also applied to measure the model uncertainty and calibration performance. A lower ECE value signifies a closer alignment between the model's confidence scores and the true probabilities of the events.

**Evaluation using Small-scale Datasets** In this experiment, we use dataset pairs of the type (ID samples vs OOD data), including CIFAR10 (Krizhevsky et al., 2009) vs SVHN (Hendrycks et al., 2021)/Tiny-ImageNet (Le & Yang, 2015) and CIFAR10 vs CIFAR10-C (Hendrycks & Dietterich, 2019). As for BNN baselines, we choose two standardized variational BNNs: BNNR (Auto-Encoding variational Bayes (Kingma & Welling, 2013) with the local reparameterization trick (Molchanov et al., 2017)) and BNNF (Flipout gradient estimator with negative evidence of lower bound loss (Wen et al., 2018)). We do not consider BNNs using sampling approaches because of their generally high computational resource requirements (Gawlikowski et al., 2021; Jospin et al., 2022). As for DEs, we aggregate five standard neural networks, trained using distinct random seeds. All models are implemented on the established VGG16 (Simonyan & Zisserman, 2015) and ResNet-18 (He et al., 2016) architectures using the CIFAR10 dataset. The number of sampled predictions for BNNs is set to $N = 5$. While the main aim of this work is to improve the uncertainty estimation performance of BNNs and DEs through the credal wrapper, it is also intriguing to compare our approach with an alternative method, Ensemble Distribution Distillation (EDD) (Malinin et al., 2019), within the evidential deep learning family. EDD aims to approximate DE predictions on the simplex by leveraging a single Dirichlet distribution. Thus, here we train EDD from the DEs under two distinct learning rate scheduler configurations: (1) EDD-Fair, which uses the same basic scheduler as BNNs and SNNs to ensure a fair comparison; and (2) EDD, which employs the cycle learning rate policy described in the original EDD paper. More implementation details are given in Appendix §B.

Table 1 reports test accuracy (ACC) and ECE values on the CIFAR10 test set and the corrupted CIFAR10 (CIFAR10-C) data as well as the OOD detection performance comparison. Regarding the CIFAR10-C dataset, which applies 15 corruption modes to the CIFAR10 instances, with 5 intensities per corruption type, Figures 2 and 3 show the OOD detection results and the ECE values of CIFAR10 vs CIFAR10-C against increased corruption intensity, respectively. The results over the 15 corruption types are averaged. Table 1 and Figure 3 demonstrate that our intersection probability exhibits comparable test ACC and ECE on ID test data, compared to the classical averaged probability. Moreover, the calibration performance on corrupted samples is consistently better, as evidenced by the lower ECE values. Table 1 and Figure 2 also demonstrate that our credal wrapper markedly and persistently enhances the EU estimation of baselines. This is evidenced by the augmented OOD detection performance on various data pairs and across disparate backbones. Compared to EDD, which applies a cycle learning rate policy, our credal wrapper still consistently achieves superior performance, as shown in Table 1 and Figure 2. Concerning EDD-Fair, we observe that fairly applying the simple learning rate scheduler leads to low prediction performance of EDD-Fair (considerably

Table 1: Performance comparison between the classical and credal wrapper version of BNN and DE, as well as EDD models. All models are implemented on VGG16/ResNet-18 backbones and trained using CIFAR10 data as ID samples. The results are from 15 runs. The best scores per metric are in bold. The results on corrupted data are averaged over all corruption types and intensities.

| | | | Prediction Performance | | | | OOD Detection Performance (%) using EU | | | |
|---|---|---|---|---|---|---|---|---|---|---|
| | | | ID Test Data | | Corrupted Data | | SVHN (OOD) | | Tiny-ImageNet (OOD) | |
| | | | ACC (%) | ECE | ACC (%) | ECE | AUROC | AUPRC | AUROC | AUPRC |
| VGG16 | BNNR | Baseline | **90.98±0.11** | 0.048±0.003 | 21.86±1.88 | 0.470±0.050 | 86.65±1.26 | 90.61±0.88 | 84.62±0.28 | 80.06±0.40 |
| | | Ours | **90.98±0.15** | **0.034±0.003** | **21.96±1.83** | **0.416±0.050** | **87.85±1.45** | **92.32±1.05** | **85.55±0.30** | **82.76±0.46** |
| | BNNF | Baseline | **90.88±0.19** | 0.055±0.003 | 23.00±1.97 | 0.498±0.066 | 86.79±0.47 | 90.76±0.55 | 84.54±0.20 | 79.91±0.35 |
| | | Ours | 90.84±0.20 | **0.043±0.003** | **23.08±1.93** | **0.452±0.068** | **87.66±0.50** | **92.26±0.51** | **85.26±0.20** | **82.33±0.30** |
| | DE | Baseline | **93.57±0.09** | **0.015±0.001** | 24.81±0.79 | 0.314±0.024 | 89.74±1.31 | 93.58±0.97 | 88.49±0.17 | 85.79±0.35 |
| | | Ours | 93.47±0.10 | 0.033±0.002 | **24.42±0.81** | 0.200±0.022 | **91.96±1.33** | **95.24±0.79** | **89.80±0.08** | **87.99±0.16** |
| | EDD | | 91.05±0.18 | 0.038±0.003 | 19.37±2.24 | **0.122±0.062** | 91.21±0.95 | 93.62±1.70 | 87.04±0.75 | 82.53±2.18 |
| ResNet-18 | BNNR | Baseline | **91.87±0.17** | 0.058±0.002 | 22.38±1.31 | 0.498±0.030 | 88.32±1.22 | 93.03±0.74 | 85.83±0.25 | 81.43±0.51 |
| | | Ours | 91.86±0.18 | **0.055±0.002** | **22.45±1.30** | **0.460±0.030** | **88.40±1.25** | **93.16±0.79** | **85.99±0.20** | **82.51±0.39** |
| | BNNF | Baseline | **91.91±0.19** | 0.057±0.002 | 22.38±1.30 | 0.498±0.024 | 88.62±0.80 | 93.26±0.52 | 85.94±0.30 | 81.64±0.34 |
| | | Ours | 91.90±0.18 | **0.055±0.002** | **22.43±1.30** | **0.464±0.024** | **88.71±0.81** | **93.41±0.51** | **86.06±0.31** | **82.69±0.27** |
| | DE | Baseline | **93.36±0.11** | **0.018±0.001** | 26.62±0.69 | 0.304±0.018 | 87.40±0.68 | 91.82±0.51 | 87.94±0.15 | 84.86±0.24 |
| | | Ours | 93.35±0.13 | 0.025±0.002 | 26.41±0.73 | **0.224±0.016** | **88.63±0.80** | **92.76±0.64** | **89.16±0.15** | **87.41±0.19** |
| | EDD | | 92.96±0.10 | 0.027±0.001 | **27.00±1.20** | 0.276±0.032 | 87.26±1.57 | 91.91±1.01 | 88.05±0.23 | 83.66±0.41 |

below the baselines) and poor EU estimation (evidenced by the lowest OOD detection values), as shown in Table 15 in the Appendix.

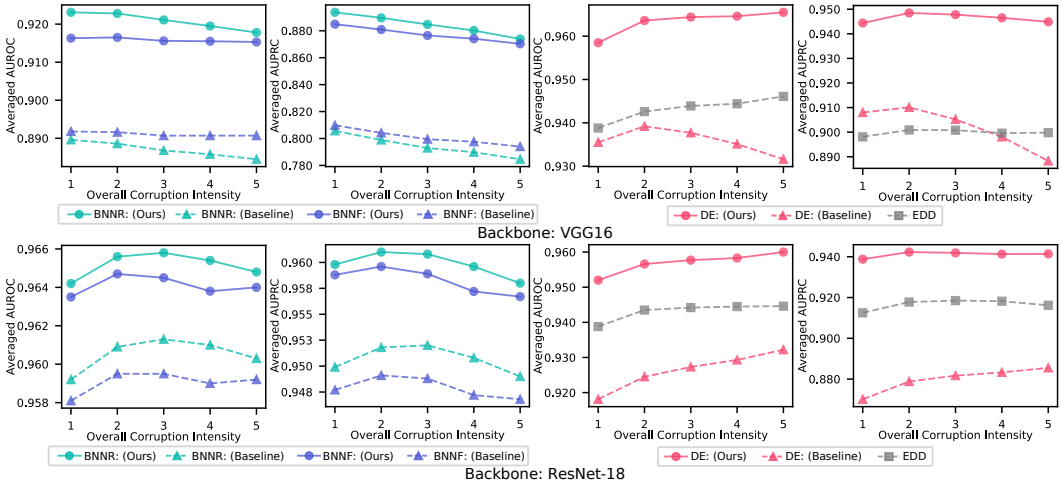


Figure 2: OOD detection using EU as the metric on CIFAR10 vs CIFAR10-C of the classical and credal wrapper version of BNNs and DE, and EDD against increased corruption intensity, using VGG16 and ResNet-18 as backbones.

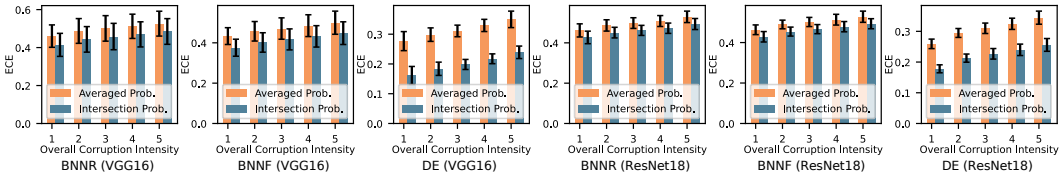


Figure 3: ECE values of BNNR, BNNF, and DE on CIFAR10-C against increased corruption intensity, using the averaged probability (Prob.) and our proposed intersection probability (Prob.). VGG16 and ResNet-18 are backbones. Results are from 15 runs.

**Evaluation using Large-scale Datasets** In this experiment, we exclusively employ DEs (combining five SNNs) to assess the quality of EU estimation of our credal wrapper on large-scale datasets and network architectures. This is because, in practice, BNNs are typically unable to scale to large

Table 2: OOD detection AUROC and AUPRC performance (%) of both the classical and credal wrapper version of DEs using EU as the metric. The results are from 15 runs, based on the ResNet-50 backbone. Best scores are in bold.

| | CIFAR10 (ID) | | | | CIFAR100 (ID) | | | | ImageNet (ID) | |
|---|---|---|---|---|---|---|---|---|---|---|
| | SVHN (OOD) | | Tiny-ImageNet (OOD) | | SVHN (OOD) | | Tiny-ImageNet (OOD) | | ImageNet-O (OOD) | |
| | AUROC | AUPRC | AUROC | AUPRC | AUROC | AUPRC | AUROC | AUPRC | AUROC | AUPRC |
| Baseline | 89.58±0.93 | 92.29±1.00 | 86.87±0.20 | 83.02±0.16 | 73.83±1.97 | 84.96±1.25 | 78.80±0.20 | 74.68±0.27 | 65.70±0.41 | 63.20±0.35 |
| Ours | **93.77±0.60** | **96.06±0.46** | **88.78±0.15** | **86.83±0.23** | **80.22±1.96** | **89.40±1.03** | **81.00±0.16** | **77.16±0.23** | **66.20±0.38** | **63.23±0.34** |

datasets and model architectures due to the high computational complexity (Mukhoti et al., 2023). For instance, training a ResNet-50-based BNN on CIFAR-10 (resized to (224, 224, 3)) failed in our experiment due to exceeding the memory capacity of a single Nvidia A100 GPU. The dataset pairs (ID vs OOD) considered include CIFAR10/CIFAR100 (Krizhevsky, 2012) vs SVHN/Tiny-ImageNet, ImageNet (Deng et al., 2009) vs ImageNet-O (Hendrycks et al., 2021), CIFAR10 vs CIFAR10-C, and CIFAR100 vs CIFAR100-C (Hendrycks & Dietterich, 2019). DEs are implemented on the well-established ResNet-50 (He et al., 2016). All input data have a shape of (224, 224, 3). More training details are given in Appendix §B. The PIA algorithm (Algorithm 1) is applied using the settings $J = 20$ and $J = 50$ to calculate the generalized entropy ($\overline{H}(\mathbb{P})$ and $\underline{H}(\mathbb{P})$) on dataset pairs involving CIFAR100 and ImageNet, respectively. Compared to classical DEs, our credal wrapper demonstrates the enhanced OOD detection across a spectrum of data pairs, as shown in Table 2, suggesting that our proposed method can consistently improve EU estimation.

**Ablation Study on Network Architectures** We also perform an ablation study using EfficientNetB2 (EffB2) (Tan & Le, 2021) and Vision Transformer Base (ViT-B) (Dosovitskiy et al., 2020) as architecture backbones, involving CIFAR10/100 vs SVHN and Tiny-ImageNet, CIFAR10 vs CIFAR10-C, and CIFAR100 vs CIFAR100-C. The key findings, presented in Table 3 and Figure 4, demonstrate that our credal wrapper approach significantly enhances the EU quality of DEs, and is robust against both the dataset pairs and the architecture backbones. Furthermore, Figure 5 shows the ECE values exhibited by DEs on both CIFAR10-C and CIFAR100-C datasets, using ResNet-50, EffB2, and ViT-B backbones. The results indicate that adopting the intersection probability as the final prediction, with its strong rationality foundations, can indeed empirically improve calibration performance (lower ECE) on the corrupted samples by using the classical averaged probability.

Table 3: OOD detection AUROC and AUPRC performance (%) of the classical and credal wrapper version of DEs using EU as the metric. Results are from 15 runs, based on EffB2 and ViT-B backbones. Best scores are in bold.

| | | CIFAR 10 (ID) | | | | CIFAR 100 (ID) | | | |
|---|---|---|---|---|---|---|---|---|---|
| | | SVHN (OOD) | | Tiny-ImageNet (OOD) | | SVHN (OOD) | | Tiny-ImageNet (OOD) | |
| | | AUROC | AUPRC | AUROC | AUPRC | AUROC | AUPRC | AUROC | AUPRC |
| EffB2 | Baseline | 95.76±0.59 | 97.43±0.47 | 92.32±0.14 | 90.72±0.22 | 87.52±1.52 | 93.81±0.80 | 85.29±0.15 | 82.98±0.24 |
| | Ours | **97.60±0.25** | **98.74±0.14** | **93.55±0.15** | **93.17±0.16** | **89.20±1.19** | **94.58±0.56** | **86.23±0.10** | **83.69±0.21** |
| ViT-B | Baseline | 77.71±1.67 | 85.82±1.14 | 82.27±0.79 | 78.85±0.81 | 81.41±1.33 | 89.00±0.96 | 81.18±0.31 | 77.46±0.49 |
| | Ours | **80.71±1.83** | **88.43±1.26** | **84.28±0.76** | **82.82±0.85** | **84.87±1.06** | **91.40±0.67** | **82.53±0.32** | **79.04±0.39** |

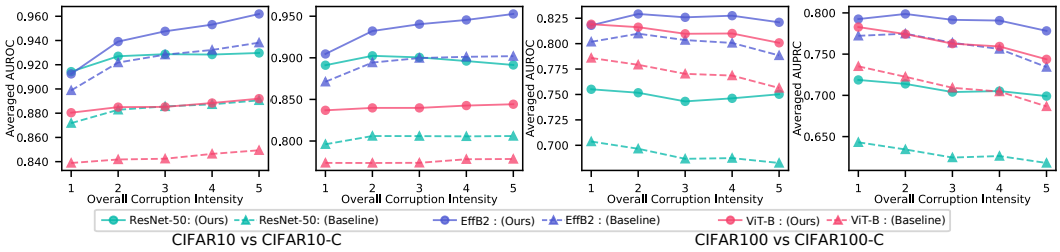


Figure 4: OOD detection performance of the classical and credal wrapper version of DEs using EU as the metric on CIFAR10/100 vs CIFAR10-C/100-C against increased corruption intensity, using ResNet-50, EffB2, and ViT-B as backbones.

**Ablation Study on Numbers of Predictive Samples in DEs** In this experiment, we train 30 ResNet-50-based SNNs individually using the CIFAR10 dataset and under different random seeds.

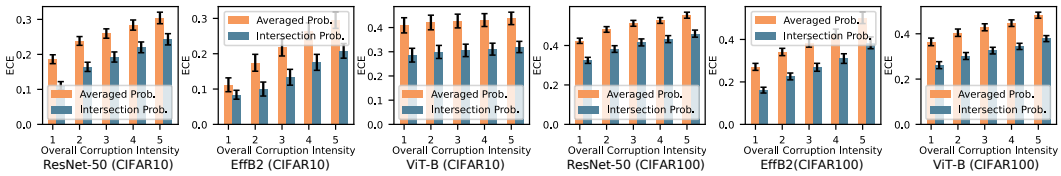


Figure 5: ECE values of DEs on CIFAR10-C and CIFAR100-C against increased corruption intensity, using the averaged probability (Prob.) and our proposed intersection probability (Prob.). ResNet-50, EffB2, and ViT-B are backbones. Results are from 15 runs.

Then, we construct DEs using different numbers of ensemble members, namely $N = 3, 5, 10, 15, 20$ and 25. Each type of DEs includes 15 instances using distinct seed combinations.

Table 4 reports OOD detection performance comparisons under different numbers of samples. The findings suggest that (i) Increasing the number of samples can indeed improve the EU estimation of our proposed credal wrapper. (ii) Compared to classical DEs, our method consistently shows superior performance on EU quantification, robustly against the number of samples. Figure 6 shows the ECE performance evaluation using different settings of $N$ on the CIFAR10-C samples. We can observe that: (i) Increasing the number of samples overall can lead to a lower ECE value; (ii) Compared to the the naive averaging DE predictions, our intersection probability consistently achieves lower ECE values on corrupted instances.

Table 4: OOD detection performance (%) comparison in DEs.

| $N$ | CIFAR10 vs SVHN | | | | CIFAR10 vs Tiny-ImageNet | | | |
|---|---|---|---|---|---|---|---|---|
| | AUROC | | AUPRC | | AUROC | | AUPRC | |
| | Baseline | Ours | Baseline | Ours | Baseline | Ours | Baseline | Ours |
| 3 | 89.64±1.16 | **91.97±1.38** | 92.13±1.12 | **94.91±1.08** | 86.31±0.24 | **87.57±0.25** | 81.76±0.40 | **85.02±0.32** |
| 5 | 89.26±1.02 | **93.50±0.79** | 91.96±0.97 | **95.79±0.70** | 86.83±0.25 | **88.65±0.25** | 83.12±0.38 | **86.77±0.37** |
| 10 | 90.54±0.72 | **95.03±0.40** | 93.22±0.70 | **96.80±0.35** | 87.75±0.13 | **89.62±0.14** | 84.99±0.25 | **88.04±0.20** |
| 15 | 90.78±0.68 | **95.31±0.47** | 93.23±0.62 | **96.91±0.43** | 88.10±0.10 | **89.94±0.10** | 85.59±0.16 | **88.44±0.13** |
| 20 | 91.09±0.50 | **95.69±0.34** | 93.49±0.48 | **97.15±0.30** | 88.33±0.08 | **90.11±0.08** | 85.96±0.11 | **88.59±0.10** |
| 25 | 91.31±0.27 | **95.84±0.15** | 93.62±0.24 | **97.24±0.12** | 88.46±0.04 | **90.22±0.05** | 86.17±0.08 | **88.72±0.07** |

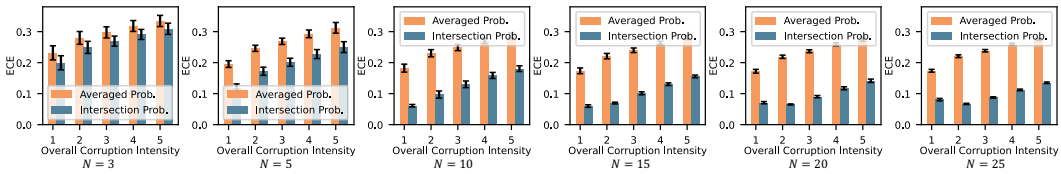


Figure 6: ECE values of DEs with various $N$ on CIFAR10-C against increased corruption intensity.

**Ablation Study on Numbers of Predictive Samples in BNNs** In this experiment, we first increase the sampling size of BNNs at prediction time, namely $N = 10$ and $N = 50$. Table 6 reports the OOD detection performance of BNNR and BNNF involving CIFAR10 (ID) vs SVHN and Tiny-ImageNet (OODs), based on the VGG16 backbone. It shows that credal wrapper consistently produces better EU estimates, as evidenced by enhanced OOD detection performance. Further, Table 12 in the Appendix reports the same comparison based on the ResNet-18 architecture, confirming those results.

Tables 4 and 6 suggest that our credal wrapper provides better uncertainty estimation than Bayesian methods, even when the latter use more samples. For instance, the OOD detection performance of traditional DEs with $N = 25$ is significantly lower than that with $N = 5$ when using our credal wrapper. Moreover, the OOD performance of our credal wrapper with $N = 10$ consistently surpasses that of conventional BNNs with $N = 50$. From this perspective, our credal wrapper can reduce the complexity as increasing the number of samples typically demands more computational resources and memory, such as the additional single models required for DEs during training and inference.

Table 5: Performance comparison when applying $N = 1000$ to the ResNet-18-based BNNR.

| | ID Performance | | CIFAR10 vs SVHN | | CIFAR10 vs Tiny-ImageNet | |
|---|---|---|---|---|---|---|
| | ACC | ECE | AUROC | AUPRC | AUROC | AUPRC |
| Baseline | 91.89±0.18 | 0.057±0.002 | 87.24±1.72 | 93.09±0.89 | 83.94±0.32 | 81.15±0.39 |
| Ours | **91.90±0.16** | **0.034±0.003** | **89.36±1.25** | **93.88±0.86** | **86.89±0.19** | **84.63±0.33** |

Additionally, we further increase the number of samples ($N = 1000$) for the ResNet18-based BNNR to explore an extreme case. Table 5 compares the test ACC and ECE values between two approaches, namely $\tilde{\boldsymbol{p}}$ and $\boldsymbol{p}^*$, as well as the OOD detection performance. Although a high sampling size is rarely

Table 6: OOD detection comparisons using EU (%) of VGG16-based BNNs.

| $N$ | Method | BNNR: CIFAR10 (ID) | | | | BNNF: CIFAR10 (ID) | | | |
|---|---|---|---|---|---|---|---|---|---|
| | | SVHN (OOD) | | Tiny-ImageNet (OOD) | | SVHN (OOD) | | Tiny-ImageNet (OOD) | |
| | | AUROC | AUPRC | AUROC | AUPRC | AUROC | AUPRC | AUROC | AUPRC |
| 10 | Baseline | 86.60±1.28 | 90.54±1.00 | 85.00±0.27 | 80.90±0.42 | 86.67±0.54 | 90.64±0.71 | 84.78±0.18 | 80.51±0.38 |
| | Ours | **88.38±1.53** | **92.61±1.12** | **86.28±0.25** | **83.88±0.32** | **88.03±0.52** | **92.55±0.52** | **85.79±0.18** | **83.29±0.28** |
| 50 | Baseline | 86.60±1.37 | 90.44±1.02 | 85.41±0.21 | 81.79±0.30 | 86.63±0.60 | 90.56±0.79 | 85.10±0.19 | 81.28±0.34 |
| | Ours | **88.90±1.65** | **92.75±1.22** | **87.17±0.26** | **85.22±0.33** | **88.60±0.56** | **92.91±0.54** | **86.61±0.21** | **84.64±0.27** |

employed in BNNs due to the inherent complexity, the results illustrate the stability of our methods and the consistent superiority of our credal wrapper compared to the BNN baseline.

**Additional Experiments** Appendix §A.1 examines the EU quantification performance of our credal wrapper using the generalized Hartley measure (Abellán & Moral, 2000), as an alternative to the difference between upper and lower entropy in eq. (4). The results demonstrate that our credal wrapper consistently enhances the EU estimation performance while being agnosticto the specific EU measure for credal sets employed. Appendix §A.2 assesses the TU estimation quality (as opposed to EU) on OOD detection benchmarks, suggesting that our credal wrapper consistently improves TU estimation as well, across the different dataset pairs, network architectures, and test settings. Appendix §A.3 presents an examination of the performance of our credal wrapper in scenarios where the ensemble member (SNN) generates overconfident predictions. The findings also show the improved uncertainty quantification of our credal wrapper. Appendix §A.4 presents uncertainty estimate plots for both ID and OOD samples across various settings, providing further qualitative evidence that our credal wrapper consistently enhances baseline uncertainty quantification. Appendix §A.5 assesses intersection probability on corrupted samples using the negative log-likelihood (NLL) metric, showing consistently improved performance with lower values across extensive test scenarios. Appendix §A.6 analyzes the effect of the hyperparameter $J$ of the PIA algorithm 1. This evaluation indicates that the proposed PIA algorithm can significantly reduce the computational complexity of estimating uncertainty in cases of high-class classification, while maintaining superior uncertainty performance on OOD detection benchmarks.

## 5 Conclusion and Future Work

**Conclusion** This paper presents an innovative approach, called a *credal wrapper*, to formulating a credal set prediction for model averaging in BNNs and DEs, capable of improving their EU and TU estimation in classification tasks. Given a limited collection of single distributions derived at prediction time from either BNNs or DEs, the proposed approach computes a lower and an upper probability bound per class, to acknowledge the epistemic uncertainty about the sought exact predictive distribution due to limited information availability. Such lower and upper probability bounds on each class induce a credal set. From such a credal prediction (the output of our wrapper), an intersection probability distribution can be derived, for which there are theoretical arguments that it is the natural way to map a credal set to a single probability.

Extensive experiments performed on several OOD detection benchmarks, including CIFAR10/100 vs SVHN/Tiny-ImageNet, CIFAR10/100 vs CIFAR10/100-C, and ImageNet vs ImageNet-O, and utilizing various network architectures (VGG16, ResNet-18/50, EfficientNet B2 and ViT Base), demonstrate that, compared to BNN and DE baselines, the proposed credal wrapper approach exhibits better uncertainty estimation and lower ECE on corrupted data.

**Limitation and Future Work** Our credal wrapper functions as a plug-and-play method for enhancing the uncertainty quantification of BNNs and DEs without requiring any additional training. However, as shown in §A.6, uncertainty quantification in this setting demands a higher computational investment. Thus, if memory usage or computational resources are strictly limited, the proposed approach may not be the optimal solution. A primary objective of our forthcoming research is to apply and benchmark our approach on safety-critical and real-world applications, such as medical image analysis.

## REPRODUCIBILITY STATEMENT

The experiment codes are included in the supplementary files and will be publicly released in an online repository upon acceptance. Detailed implementation description is provided in §B.

## REFERENCES


Taiga Abe, Estefany Kelly Buchanan, Geoff Pleiss, Richard Zemel, and John P Cunningham. Deep ensembles work, but are they necessary? *Advances in Neural Information Processing Systems*, 35:33646–33660, 2022.

Joaquín Abellán and Serafín Moral. A non-specificity measure for convex sets of probability distributions. *International journal of uncertainty, fuzziness and knowledge-based systems*, 8(03): 357–367, 2000.

Joaquín Abellán, George J Klir, and Serafín Moral. Disaggregated total uncertainty measure for credal sets. *International Journal of General Systems*, 35(1):29–44, 2006.

Neil Band, Tim GJ Rudner, Qixuan Feng, Angelos Filos, Zachary Nado, Michael W Dusenberry, Ghassen Jerfel, Dustin Tran, and Yarin Gal. Benchmarking Bayesian deep learning on diabetic retinopathy detection tasks. In *Proceedings of Conference on Neural Information Processing Systems Datasets and Benchmarks Track (Round 2)*, 2021.

Charles Blundell, Julien Cornebise, Koray Kavukcuoglu, and Daan Wierstra. Weight uncertainty in neural network. In *Proceedings of the International Conference on Machine Learning*, pp. 1613–1622. PMLR, 2015.

Andrés Cano and Serafin Moral. Using probability trees to compute marginals with imprecise probabilities. *International Journal of Approximate Reasoning*, 29(1):1–46, 2002.

Michele Caprio, Souradeep Dutta, Kuk Jin Jang, Vivian Lin, Radoslav Ivanov, Oleg Sokolsky, and Insup Lee. Credal bayesian deep learning. *Transactions on Machine Learning Research*, 2024. ISSN 2835-8856. URL `https://openreview.net/forum?id=4NHF9AC5ui`.

Bertrand Charpentier, Daniel Zügner, and Stephan Günnemann. Posterior network: Uncertainty estimation without OOD samples via density-based pseudo-counts. *Advances in neural information processing systems*, 33:1356–1367, 2020.

Alain Chateauneuf and Jean-Yves Jaffray. Some characterizations of lower probabilities and other monotone capacities through the use of möbius inversion. *Mathematical social sciences*, 17(3): 263–283, 1989.

Giorgio Corani and Marco Zaffalon. Learning reliable classifiers from small or incomplete data sets: The naive credal classifier 2. *Journal of Machine Learning Research*, 9(4), 2008.

Giorgio Corani, Alessandro Antonucci, and Marco Zaffalon. Bayesian networks with imprecise probabilities: Theory and application to classification. *Data Mining: Foundations and Intelligent Paradigms: Volume 1: Clustering, Association and Classification*, pp. 49–93, 2012.

Fabio Cuzzolin. On the credal structure of consistent probabilities. In *European Workshop on Logics in Artificial Intelligence*, pp. 126–139. Springer, 2008.

Fabio Cuzzolin. Credal semantics of bayesian transformations in terms of probability intervals. *IEEE Transactions on Systems, Man, and Cybernetics, Part B (Cybernetics)*, 40(2):421–432, 2009.

Fabio Cuzzolin. *The geometry of uncertainty: The geometry of imprecise probabilities*. Springer Nature, 2020.

Fabio Cuzzolin. The intersection probability: betting with probability intervals. *arXiv preprint arXiv:2201.01729*, 2022.

Fabio Cuzzolin. Uncertainty measures: A critical survey. *Information Fusion*, pp. 102609, 2024.

Erik Daxberger, Agustinus Kristiadi, Alexander Immer, Runa Eschenhagen, Matthias Bauer, and Philipp Hennig. Laplace Redux - Effortless Bayesian Deep Learning. In M. Ranzato, A. Beygelzimer, Y. Dauphin, P.S. Liang, and J. Wortman Vaughan (eds.), *Advances in Neural Information Processing Systems*, volume 34, pp. 20089–20103. Curran Associates, Inc., 2021. URL https://proceedings.neurips.cc/paper_files/paper/2021/file/a7c9585703d275249f30a088cebba0ad-Paper.pdf.

Luis M. De Campos, Juan F. Huete, and Serafin Moral. Probability intervals: A tool for uncertain reasoning. *International Journal of Uncertainty, Fuzziness and Knowledge-Based Systems*, 02: 167–196, June 1994. ISSN 0218-4885, 1793-6411. doi: 10.1142/S0218488594000146.

Bruno De Finetti. *Theory of probability: A critical introductory treatment*, volume 6. John Wiley & Sons, 2017.

Jia Deng, Wei Dong, Richard Socher, Li-Jia Li, Kai Li, and Li Fei-Fei. Imagenet: A large-scale hierarchical image database. In *2009 IEEE conference on computer vision and pattern recognition*, pp. 248–255. Ieee, 2009.

Stefan Depeweg, Jose-Miguel Hernandez-Lobato, Finale Doshi-Velez, and Steffen Udluft. Decomposition of uncertainty in Bayesian deep learning for efficient and risk-sensitive learning. In *International Conference on Machine Learning*, pp. 1184–1193. PMLR, 2018.

Alexey Dosovitskiy, Lucas Beyer, Alexander Kolesnikov, Dirk Weissenborn, Xiaohua Zhai, Thomas Unterthiner, Mostafa Dehghani, Matthias Minderer, Georg Heigold, Sylvain Gelly, et al. An image is worth 16x16 words: Transformers for image recognition at scale. *arXiv preprint arXiv:2010.11929*, 2020.

Didier Dubois and Henri Prade. Consonant approximations of belief functions. *International Journal of Approximate Reasoning*, 4(5-6):419–449, 1990.

Michael Dusenberry, Ghassen Jerfel, Yeming Wen, Yian Ma, Jasper Snoek, Katherine Heller, Balaji Lakshminarayanan, and Dustin Tran. Efficient and scalable Bayesian neural nets with rank-1 factors. In *International conference on machine learning*, pp. 2782–2792. PMLR, 2020.

Yarin Gal and Zoubin Ghahramani. Dropout as a Bayesian approximation: Representing model uncertainty in deep learning. In *Proceedings of the International Conference on Machine Learning*, pp. 1050–1059. PMLR, 2016.

Jakob Gawlikowski, Cedrique Rovile Njieutcheu Tassi, Mohsin Ali, Jongseok Lee, Matthias Humt, Jianxiang Feng, Anna Kruspe, Rudolph Triebel, Peter Jung, Ribana Roscher, et al. A survey of uncertainty in deep neural networks. *ArXiv Preprint ArXiv:2107.03342*, 2021.

Chuan Guo, Geoff Pleiss, Yu Sun, and Kilian Q Weinberger. On calibration of modern neural networks. In *International conference on machine learning*, pp. 1321–1330. PMLR, 2017.

Peijun Guo and Hideo Tanaka. Decision making with interval probabilities. *European Journal of Operational Research*, 203(2):444–454, 2010.

Fredrik K Gustafsson, Martin Danelljan, and Thomas B Schon. Evaluating scalable Bayesian deep learning methods for robust computer vision. In *Proceedings of the IEEE/CVF conference on computer vision and pattern recognition workshops*, pp. 318–319, 2020.

Bobby He, Balaji Lakshminarayanan, and Yee Whye Teh. Bayesian deep ensembles via the neural tangent kernel. *Advances in neural information processing systems*, 33:1010–1022, 2020.

Kaiming He, Xiangyu Zhang, Shaoqing Ren, and Jian Sun. Deep residual learning for image recognition. In *Proceedings of the IEEE conference on computer vision and pattern recognition*, pp. 770–778, 2016.

Dan Hendrycks and Thomas Dietterich. Benchmarking neural network robustness to common corruptions and perturbations. *Proceedings of the International Conference on Learning Representations*, 2019.

Dan Hendrycks and Kevin Gimpel. A baseline for detecting misclassified and out-of-distribution examples in neural networks. *arXiv preprint arXiv:1610.02136*, 2016.

Dan Hendrycks, Kevin Zhao, Steven Basart, Jacob Steinhardt, and Dawn Song. Natural adversarial examples. In *Proceedings of the IEEE/CVF Conference on Computer Vision and Pattern Recognition*, pp. 15262–15271, 2021.

Marius Hobbhahn, Agustinus Kristiadi, and Philipp Hennig. Fast predictive uncertainty for classification with Bayesian deep networks. In James Cussens and Kun Zhang (eds.), *Proceedings of the Thirty-Eighth Conference on Uncertainty in Artificial Intelligence*, volume 180 of *Proceedings of Machine Learning Research*, pp. 822–832. PMLR, 01–05 Aug 2022. URL https://proceedings.mlr.press/v180/hobbhahn22a.html.

Matthew D Hoffman, Andrew Gelman, et al. The No-U-Turn sampler: adaptively setting path lengths in Hamiltonian Monte Carlo. *J. Mach. Learn. Res.*, 15(1):1593–1623, 2014.

Eyke Hüllermeier and Willem Waegeman. Aleatoric and epistemic uncertainty in machine learning: An introduction to concepts and methods. *Machine Learning*, 110(3):457–506, 2021.

Eyke Hüllermeier, Sébastien Destercke, and Mohammad Hossein Shaker. Quantification of credal uncertainty in machine learning: A critical analysis and empirical comparison. In *Proceedings of the Uncertainty in Artificial Intelligence*, pp. 548–557. PMLR, 2022.

Laurent Valentin Jospin, Hamid Laga, Farid Boussaid, Wray Buntine, and Mohammed Bennamoun. Hands-on Bayesian neural networks—A tutorial for deep learning users. *IEEE Computational Intelligence Magazine*, 17(2):29–48, 2022.

Mira Juergens, Nis Meinert, Viktor Bengs, Eyke Hüllermeier, and Willem Waegeman. Is epistemic uncertainty faithfully represented by evidential deep learning methods? In *Forty-first International Conference on Machine Learning*, 2024.

Alex Kendall and Yarin Gal. What uncertainties do we need in Bayesian deep learning for computer vision? *Advances in Neural Information Processing Systems*, 30, 2017.

Diederik P Kingma and Max Welling. Auto-encoding variational Bayes. *arXiv preprint arXiv:1312.6114*, 2013.

Alex Krizhevsky. Learning multiple layers of features from tiny images. *University of Toronto*, 05 2012.

Alex Krizhevsky, Vinod Nair, and Geoffrey Hinton. CIFAR-10 (Canadian Institute For Advanced Research). Technical report, CIFAR, 2009. URL https://www.cs.toronto.edu/~kriz/cifar.html.

David Krueger, Chin-Wei Huang, Riashat Islam, Ryan Turner, Alexandre Lacoste, and Aaron Courville. Bayesian hypernetworks. *ArXiv Preprint ArXiv:1710.04759*, 2017.

Henry E Kyburg Jr. Bayesian and non-bayesian evidential updating. *Artificial intelligence*, 31(3): 271–293, 1987.

Balaji Lakshminarayanan, Alexander Pritzel, and Charles Blundell. Simple and scalable predictive uncertainty estimation using deep ensembles. *Advances in Neural Information Processing Systems*, 30, 2017.

Antonis Lambrou, Harris Papadopoulos, and Alex Gammerman. Reliable confidence measures for medical diagnosis with evolutionary algorithms. *IEEE Transactions on Information Technology in Biomedicine*, 15(1):93–99, 2010.

Ya Le and Xuan Yang. Tiny imagenet visual recognition challenge. *CS 231N*, 7(7):3, 2015.

Isaac Levi. *The enterprise of knowledge: An essay on knowledge, credal probability, and chance*. MIT press, 1980.

Jeremiah Liu, Zi Lin, Shreyas Padhy, Dustin Tran, Tania Bedrax Weiss, and Balaji Lakshminarayanan. Simple and principled uncertainty estimation with deterministic deep learning via distance awareness. *Advances in Neural Information Processing Systems*, 33:7498–7512, 2020.

Andrey Malinin and Mark Gales. Predictive uncertainty estimation via prior networks. *Advances in neural information processing systems*, 31, 2018.

Andrey Malinin and Mark Gales. Reverse kl-divergence training of prior networks: Improved uncertainty and adversarial robustness. *Advances in Neural Information Processing Systems*, 32, 2019.

Andrey Malinin, Bruno Mlodozeniec, and Mark Gales. Ensemble distribution distillation. In *International Conference on Learning Representations*, 2019.

Denis D Mauá, Fabio G Cozman, Diarmaid Conaty, and Cassio P Campos. Credal sum-product networks. In *Proceedings of the Tenth International Symposium on Imprecise Probability: Theories and Applications*, pp. 205–216. PMLR, 2017.

Hendrik A Mehrtens, Alexander Kurz, Tabea-Clara Bucher, and Titus J Brinker. Benchmarking common uncertainty estimation methods with histopathological images under domain shift and label noise. *Medical Image Analysis*, 89:102914, 2023.

Aryan Mobiny, Pengyu Yuan, Supratik K Moulik, Naveen Garg, Carol C Wu, and Hien Van Nguyen. Dropconnect is effective in modeling uncertainty of Bayesian deep networks. *Scientific Reports*, 11(1):1–14, 2021.

Dmitry Molchanov, Arsenii Ashukha, and Dmitry Vetrov. Variational dropout sparsifies deep neural networks. In *Proceedings of the International Conference on Machine Learning*, pp. 2498–2507. PMLR, 2017.

Serafín Moral-García and Joaquín Abellán. Credal sets representable by reachable probability intervals and belief functions. *International Journal of Approximate Reasoning*, 129:84–102, 2021.

Bálint Mucsányi, Michael Kirchhof, and Seong Joon Oh. Benchmarking uncertainty disentanglement: Specialized uncertainties for specialized tasks. *arXiv preprint arXiv:2402.19460*, 2024.

Jishnu Mukhoti, Andreas Kirsch, Joost van Amersfoort, Philip HS Torr, and Yarin Gal. Deep deterministic uncertainty: A new simple baseline. In *Proceedings of the IEEE/CVF Conference on Computer Vision and Pattern Recognition*, pp. 24384–24394, 2023.

Radford M Neal et al. MCMC using Hamiltonian dynamics. *Handbook of Markov Chain Monte Carlo*, 2(11):2, 2011.

Hung T Nguyen. On random sets and belief functions. *Journal of Mathematical Analysis and Applications*, 65(3):531–542, 1978.

Jeremy Nixon, Michael W Dusenberry, Linchuan Zhang, Ghassen Jerfel, and Dustin Tran. Measuring calibration in deep learning. In *CVPR workshops*, volume 2, 2019.

Yaniv Ovadia, Emily Fertig, Jie Ren, Zachary Nado, David Sculley, Sebastian Nowozin, Joshua Dillon, Balaji Lakshminarayanan, and Jasper Snoek. Can you trust your model's uncertainty? evaluating predictive uncertainty under dataset shift. *Advances in neural information processing systems*, 32, 2019.

Nicolas Papernot, Patrick McDaniel, Somesh Jha, Matt Fredrikson, Z Berkay Celik, and Ananthram Swami. The limitations of deep learning in adversarial settings. In *2016 IEEE European symposium on security and privacy (EuroS&P)*, pp. 372–387. IEEE, 2016.

Tim GJ Rudner, Zonghao Chen, Yee Whye Teh, and Yarin Gal. Tractable function-space variational inference in bayesian neural networks. *Advances in Neural Information Processing Systems*, 35: 22686–22698, 2022.

Yusuf Sale, Michele Caprio, and Eyke Höllermeier. Is the volume of a credal set a good measure for epistemic uncertainty? In *Uncertainty in Artificial Intelligence*, pp. 1795–1804. PMLR, 2023a.

Yusuf Sale, Michele Caprio, and Eyke Hüllermeier. Is the volume of a credal set a good measure for epistemic uncertainty? In *Accepted for Conference on Uncertainty in Artificial Intelligence (UAI 2023)*, pp. 0–12, 2023b.

Robin Senge, Stefan Bösner, Krzysztof Dembczyński, Jörg Haasenritter, Oliver Hirsch, Norbert Donner-Banzhoff, and Eyke Hüllermeier. Reliable classification: Learning classifiers that distinguish aleatoric and epistemic uncertainty. *Information Sciences*, 255:16–29, 2014.

Mohammad Hossein Shaker and Eyke Hüllermeier. Ensemble-based uncertainty quantification: Bayesian versus credal inference. In *PROCEEDINGS 31. WORKSHOP COMPUTATIONAL INTELLIGENCE*, volume 25, pp. 63, 2021.

K Simonyan and A Zisserman. Very deep convolutional networks for large-scale image recognition. In *3rd International Conference on Learning Representations (ICLR 2015)*. Computational and Biological Learning Society, 2015.

Mingxing Tan and Quoc Le. Efficientnetv2: Smaller models and faster training. In Marina Meila and Tong Zhang (eds.), *Proceedings of the 38th International Conference on Machine Learning*, volume 139 of *Proceedings of Machine Learning Research*, pp. 10096–10106. PMLR, 18–24 Jul 2021. URL https://proceedings.mlr.press/v139/tan21a.html.

Bjørnar Tessem. Interval probability propagation. *International Journal of Approximate Reasoning*, 7(3-4):95–120, 1992.

Ba-Hien Tran, Simone Rossi, Dimitrios Milios, and Maurizio Filippone. All you need is a good functional prior for Bayesian deep learning. *ArXiv Preprint ArXiv:2011.12829*, 2020.

Dennis Thomas Ulmer, Christian Hardmeier, and Jes Frellsen. Prior and posterior networks: A survey on evidential deep learning methods for uncertainty estimation. *Transactions on Machine Learning Research*, 2023.

Pauli Virtanen, Ralf Gommers, Travis E. Oliphant, Matt Haberland, Tyler Reddy, David Cournapeau, Evgeni Burovski, Pearu Peterson, Warren Weckesser, Jonathan Bright, Stéfan J. van der Walt, Matthew Brett, Joshua Wilson, K. Jarrod Millman, Nikolay Mayorov, Andrew R. J. Nelson, Eric Jones, Robert Kern, Eric Larson, C J Carey, İlhan Polat, Yu Feng, Eric W. Moore, Jake VanderPlas, Denis Laxalde, Josef Perktold, Robert Cimrman, Ian Henriksen, E. A. Quintero, Charles R. Harris, Anne M. Archibald, Antônio H. Ribeiro, Fabian Pedregosa, Paul van Mulbregt, and SciPy 1.0 Contributors. SciPy 1.0: Fundamental Algorithms for Scientific Computing in Python. *Nature Methods*, 17:261–272, 2020. doi: 10.1038/s41592-019-0686-2.

Peter Walley. Statistical reasoning with imprecise probabilities. 1991.

Anton Wallner. Maximal number of vertices of polytopes defined by f-probabilities. In *ISIPTA*, pp. 388–395. Citeseer, 2005.

Tonghui Wei, Wenjie Zuo, Hongwei Zheng, and Feng Li. Slope hybrid reliability analysis considering the uncertainty of probability-interval using three-parameter weibull distribution. *Natural Hazards*, 105:565–586, 2021.

Yeming Wen, Paul Vicol, Jimmy Ba, Dustin Tran, and Roger Grosse. Flipout: Efficient pseudo-independent weight perturbations on mini-batches. In *Proceedings of the International Conference on Learning Representations*, 2018. URL https://openreview.net/forum?id=rJNpifWAb.

Andrew G Wilson and Pavel Izmailov. Bayesian deep learning and a probabilistic perspective of generalization. *Advances in neural information processing systems*, 33:4697–4708, 2020.

Ronald R Yager and Vladik Kreinovich. Decision making under interval probabilities. *International Journal of Approximate Reasoning*, 22(3):195–215, 1999.

Lotfi Asker Zadeh. Fuzzy sets as a basis for a theory of possibility. *Fuzzy sets and systems*, 1(1): 3–28, 1978.

Marco Zaffalon. The naive credal classifier. *Journal of statistical planning and inference*, 105(1): 5–21, 2002.

Jindi Zhang, Yang Lou, Jianping Wang, Kui Wu, Kejie Lu, and Xiaohua Jia. Evaluating adversarial attacks on driving safety in vision-based autonomous vehicles. *IEEE Internet of Things Journal*, 9(5):3443–3456, 2021.

Dengyong Zhou, Sumit Basu, Yi Mao, and John Platt. Learning from the wisdom of crowds by minimax entropy. *Advances in Neural Information Processing Systems*, 25, 2012.

# A Additional Experiments

## A.1 Generalized Hartley Measure for EU Estimation of Credal Wrapper

In this section, we evaluate the EU quantification performance of our credal wrapper using the generalized Hartley (GH) measure (Abellán & Moral, 2000), and briefly discuss the interpretation of the generalized entropy and the GH measure in uncertainty quantification of the credal set.

**Definition and Implementation** The generalized Hartley measure (Abellán & Moral, 2000; Hüllermeier & Waegeman, 2021), $\text{GH}(\mathbb{P})$, captures the non-specificity across the distributions in the credal set, and can be seen as a proxy for its volume (Hüllermeier & Waegeman, 2021; Sale et al., 2023a) Mathematically, $\text{GH}(\mathbb{P})$ calculates the expectation of the Hartley measure over all possible subsets $\mathbb{B}$ on the target space $\mathbb{Y}$, as follows (Abellán & Moral, 2000):

$$\text{GH}(\mathbb{P}) = \sum_{\mathbb{B} \subseteq \mathbb{Y}} m_{\mathbb{P}}(\mathbb{B}) \cdot \log_2(|\mathbb{B}|), \tag{12}$$

in which $m_{\mathbb{P}}$ denotes the mass assignment function associated to a credal set $\mathbb{P}$ and $|\mathbb{B}|$ indicates the cardinality of $\mathbb{B}$. $m_{\mathbb{P}}(\mathbb{B})$ can be computed using the Möbius inverse of the capacity function $\nu_{\mathbb{P}}$ (Chateauneuf & Jaffray, 1989) as follows:

$$m_{\mathbb{P}}(\mathbb{B}) = \sum_{\mathbb{A} \subseteq \mathbb{B}} (-1)^{|\mathbb{B} \setminus \mathbb{A}|} \nu_{\mathbb{P}}(\mathbb{A}), \tag{13}$$

where $\mathbb{B} \setminus \mathbb{A} = y | y \in \mathbb{B}$ and $y \notin \mathbb{A}$ and $\nu_{\mathbb{P}}$ describes the lower probability of all possible subsets $\mathbb{A} \subseteq \mathbb{B}$. GH Measure is computationally complex to compute. However, in our case, the lower probability $\nu_{\mathbb{P}}(\mathbb{A})$ associated with the predicted credal set can be readily computed as follows:

$$\nu_{\mathbb{P}}(\mathbb{A}) = \max\left( \sum_{y_j \in \mathbb{A}} p_{L_j}, 1 - \sum_{y_j \notin \mathbb{A}} p_{U_j} \right), \tag{14}$$

where $p_L$ and $p_U$ are the lower and upper probability values per class in the defined credal set.

**Experimental Validation** In this ablation study, we evaluate on EU estimation quality of our credal wrapper using $\text{GH}(\mathbb{P})$ measure. Table 7 reports OOD detection performance tested on CIFAR10 (ID) vs SVHN (OOD) and Tiny-ImageNet (OOD). All models are implemented on the VGG16 backbones. The results demonstrate that our credal wrapper consistently enhances EU estimation performance and is agnostic in the sense that it can accommodate any EU measure for credal sets.

Table 7: OOD detection AUROC and AUPRC performance (%) comparison between classical and credal wrapper of BNNs and DEs using EU. The results are from 15 runs.

| Model | | | EU | SVHN (OOD) | | Tiny-ImageNet (OOD) | |
|---|---|---|---|---|---|---|---|
| | | | | AUROC | AUPRC | AUROC | AUPRC |
| VGG16 | BNNR | Baseline | $H(\tilde{\boldsymbol{p}}) - \tilde{H}(\boldsymbol{p})$ | 86.65±1.26 | 90.61±0.88 | 84.62±0.28 | 80.06±0.40 |
| | | Ours | $\text{GH}(\mathbb{P})$ | **87.24±1.32** | **91.54±0.97** | **84.88±0.28** | **81.05±0.37** |
| | BNNF | Baseline | $H(\tilde{\boldsymbol{p}}) - \tilde{H}(\boldsymbol{p})$ | 86.79±0.47 | 90.76±0.55 | 84.54±0.20 | 79.91±0.35 |
| | | Ours | $\text{GH}(\mathbb{P})$ | **87.22±0.45** | **91.49±0.49** | **84.72±0.20** | **80.72±0.32** |
| | DEs | Baseline | $H(\tilde{\boldsymbol{p}}) - \tilde{H}(\boldsymbol{p})$ | 89.74±1.31 | 93.58±0.97 | 88.49±0.17 | 85.79±0.35 |
| | | Ours | $\text{GH}(\mathbb{P})$ | **90.37±1.33** | **94.21±0.89** | **88.98±0.13** | **86.88±0.26** |

**Further Discussion on Different Uncertainty Measures** Given a credal set $\mathbb{P}$, it was suggested to assume the following representation to express the uncertainty (Abellán & Moral, 2000; Hüllermeier & Waegeman, 2021):

$$\text{TU}(\mathbb{P}) = \text{EU}(\mathbb{P}) + \text{AU}(\mathbb{P}). \tag{15}$$

As a result, given $\text{TU}(\mathbb{P})$ and a generalized measure of aleatoric uncertainty (conflict) $\text{AU}(\mathbb{P})$, a generalized measure of epistemic uncertainty (non-specificity) $\text{EU}(\mathbb{P})$ can be derived via disaggregation as $\text{EU}(\mathbb{P}) = \text{TU}(\mathbb{P}) - \text{AU}(\mathbb{P})$. The lower entropy $\underline{H}(\mathbb{P})$ applied in our work indicates the lower bound of the (aleatoric) uncertainty that remains even when all epistemic uncertainty is removed, i.e., when $\mathbb{P}$ is reduced to a single distribution $\boldsymbol{p} \in \mathbb{P}$. From this perspective, $\underline{H}(\mathbb{P})$ corresponds in fact to the natural measure of irreducible (aleatoric) uncertainty. Study (Abellán et al., 2006) justifies the use of upper entropy as a global uncertainty measure for credal sets. As for the

epistemic uncertainty, the difference $\overline{H}(\mathbb{P}) - \underline{H}(\mathbb{P})$ appears to be reasonable and refers to the size of the set of candidate entropies $[\underline{H}(\mathbb{P}), \overline{H}(\mathbb{P})]$, quantifying uncertainty about the aleatoric uncertainty $H(\boldsymbol{p})$ of $\boldsymbol{p}$. Different from $\overline{H}(\mathbb{P}) - \underline{H}(\mathbb{P})$ in EU estimation, the $\text{GH}(\mathbb{P})$ measures the size of the set of candidate probabilities, and hence refers to uncertainty or imprecision about the ground-truth probability. For further discussions on the different measures and their corresponding strengths and weaknesses in measuring predictive uncertainty, we kindly refer to (Hüllermeier et al., 2022).

### A.2 Total Uncertainty Estimation Evaluation on OOD Detection Benchmarks

In this section, we assess the total uncertainty (TU) estimation quality (as opposed to EU) of our credal wrapper on various OOD detection benchmarks. Tables 8, 9, 10, 11, 12, and Figures 7, 8 show that our credal wrapper can improve the quality of TU estimation as well, across different dataset pairs, network architectures, and test settings.

Table 8: OOD detection AUROC and AUPRC performance (%) comparison between the classical and credal wrapper version of BNNs and DEs, using TU as the uncertainty metric. All models are implemented on VGG16/ResNet-18 backbones and tested on CIFAR10 (ID) vs SVHN (OOD) and Tiny-ImageNet (OOD). The results are from 15 runs. The best scores are in bold.

| | | ResNet-18: CIFAR10 (OOD) | | | | VGG16: CIFAR10 (OOD) | | | |
|---|---|---|---|---|---|---|---|---|---|
| | | SVHN (OOD) | | Tiny-ImageNet (OOD) | | SVHN (OOD) | | Tiny-ImageNet (OOD) | |
| | | AUROC | AUPRC | AUROC | AUPRC | AUROC | AUPRC | AUROC | AUPRC |
| BNNR | Baseline | 88.18±1.30 | 92.68±0.86 | 86.40±0.24 | 83.16±0.40 | 88.57±1.47 | 93.26±1.08 | 85.50±0.31 | 82.60±0.41 |
| | Ours | **88.36±1.30** | **92.95±0.87** | **86.52±0.22** | **83.66±0.38** | **88.79±1.57** | **93.44±1.14** | **85.89±0.31** | **83.53±0.43** |
| BNNF | Baseline | 88.43±0.83 | 92.90±0.51 | 86.45±0.33 | 83.22±0.33 | 88.32±0.50 | 93.06±0.51 | 85.30±0.20 | 82.32±0.30 |
| | Ours | **88.65±0.81** | **93.19±0.51** | **86.58±0.32** | **83.75±0.31** | **88.47±0.52** | **93.27±0.52** | **85.62±0.20** | **83.23±0.28** |
| DE | Baseline | 88.47±0.80 | 92.82±0.64 | 88.96±0.14 | 87.22±0.18 | 91.20±1.29 | 94.87±0.78 | 89.55±0.08 | 87.89±0.14 |
| | Ours | **88.98±0.86** | **93.13±0.70** | **89.53±0.14** | **88.23±0.17** | **92.12±1.32** | **95.41±0.75** | **90.00±0.07** | **88.49±0.17** |

Table 9: OOD detection AUROC and AUPRC performance (%) of both the classical and credal wrapper version of DEs using TU as the metric. The results are from 15 runs, based on the ResNet-50 backbone. The best scores are in bold.

| | CIFAR10 (ID) | | | | CIFAR100 (ID) | | | | ImageNet (ID) | |
|---|---|---|---|---|---|---|---|---|---|---|
| | SVHN (OOD) | | Tiny-ImageNet (OOD) | | SVHN (OOD) | | Tiny-ImageNet (OOD) | | ImageNet-O (OOD) | |
| | AUROC | AUPRC | AUROC | AUPRC | AUROC | AUPRC | AUROC | AUPRC | AUROC | AUPRC |
| Baseline | 94.80±0.43 | 97.26±0.29 | 88.80±0.19 | 87.21±0.29 | 78.53±1.94 | 88.83±1.01 | 80.75±0.15 | 77.65±0.19 | 50.20±0.07 | 50.44±0.06 |
| Ours | **95.44±0.37** | **97.57±0.23** | **89.30±0.17** | **87.97±0.25** | **80.71±1.96** | **89.97±0.99** | **81.46±0.14** | **78.29±0.17** | **54.87±0.08** | **52.27±0.05** |

Table 10: OOD detection AUROC and AUPRC performance (%) of both the classical and credal wrapper version of DEs using TU as the metric. Results are from 15 runs, based on EffB2 and ViT-B backbones. The best scores are in bold.

| | | CIFAR10 (ID) | | | | CIFAR100 (ID) | | | |
|---|---|---|---|---|---|---|---|---|---|
| | | SVHN (OOD) | | Tiny-ImageNet (OOD) | | SVHN (OOD) | | Tiny-ImageNet (OOD) | |
| | | AUROC | AUPRC | AUROC | AUPRC | AUROC | AUPRC | AUROC | AUPRC |
| EffB2 | Baseline | 97.55±0.27 | 98.78±0.16 | 93.41±0.15 | 93.01±0.17 | 88.46±1.33 | 94.40±0.59 | 86.45±0.10 | **84.88±0.14** |
| | Ours | **97.91±0.21** | **98.98±0.10** | **93.74±0.15** | **93.55±0.16** | **89.35±1.20** | **94.83±0.52** | **86.61±0.09** | 84.87±0.12 |
| ViT-B | Baseline | 79.80±1.75 | 87.97±1.17 | 83.81±0.81 | 81.67±0.89 | 84.10±1.12 | 91.41±0.72 | 82.64±0.28 | 79.94±0.43 |
| | Ours | **81.08±1.82** | **88.48±1.48** | **84.62±0.75** | **82.82±0.85** | **85.40±1.05** | **92.02±0.70** | **83.06±0.29** | **80.34±0.41** |

### A.3 Ablation Study on Overconfidence Regime

In this section, we examine the performance of our credal wrapper in scenarios where the ensemble member (SNN) generates overconfident predictions. In our credal wrapper framework, overconfidence in one of the predictions would stretch the resulting credal set. This is because the upper and lower probability bounds over classes are derived via a max/min operation in eq. (5). For instance,

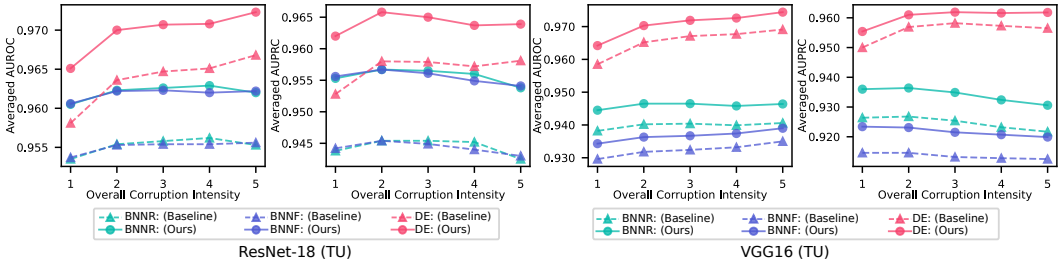


Figure 7: OOD detection using TU as metric on CIFAR10 vs CIFAR10-C of both the classical and credal wrapper version BNNs and DE against increased corruption intensity, using VGG16 and ResNet-18 as backbones.

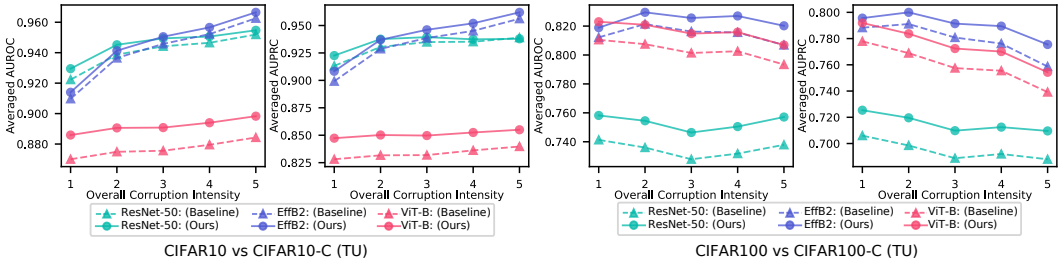


Figure 8: OOD detection using TU as the metric on CIFAR10/100 vs CIFAR10-C/100-C of both the classical and credal wrapper version of DEs against increased corruption intensity, using ResNet-50, EffB2, and ViT-B as backbones.

Table 11: Ablation study on numbers of predictive samples in DEs: OOD detection AUROC and AUPRC performance (%) of both the classical and credal wrapper version of DEs using TU as uncertainty metrics, involving CIFAR10 (ID) vs SVHN (OOD) and Tiny-ImageNet (OOD). The results are from 15 runs. The best scores are in bold.

| $N$ | CIFAR10 vs SVHN | | | | CIFAR10 vs Tiny-ImageNet | | | |
|---|---|---|---|---|---|---|---|---|
| | AUROC | | AUPRC | | AUROC | | AUPRC | |
| | Baseline | Ours | Baseline | Ours | Baseline | Ours | Baseline | Ours |
| 3 | 94.30±0.99 | **94.68±1.01** | 97.03±0.62 | **97.21±0.65** | 88.24±0.23 | **88.54±0.23** | 86.46±0.33 | **86.98±0.32** |
| 5 | 94.78±0.54 | **95.40±0.55** | 97.19±0.38 | **97.49±0.40** | 88.71±0.25 | **89.17±0.26** | 87.10±0.37 | **87.86±0.37** |
| 10 | 95.47±0.34 | **96.18±0.31** | 97.61±0.23 | **97.91±0.23** | 89.27±0.13 | **89.86±0.14** | 87.90±0.19 | **88.63±0.19** |
| 15 | 95.55±0.32 | **96.25±0.37** | 97.63±0.23 | **97.88±0.29** | 89.48±0.08 | **90.11±0.10** | 88.19±0.12 | **88.87±0.12** |
| 20 | 95.72±0.23 | **96.46±0.26** | 97.74±0.15 | **97.98±0.23** | 89.60±0.07 | **90.24±0.08** | 88.34±0.09 | **88.95±0.11** |
| 25 | 95.80±0.12 | **96.53±0.12** | 97.78±0.08 | **98.01±0.10** | 89.67±0.04 | **90.32±0.05** | 88.42±0.05 | **89.01±0.07** |

Table 12: Ablation study on numbers of predictive samples in BNNs: OOD detection AUROC and AUPRC performance (%) of both the classical and credal wrapper version of BNNs with increased number of samples, involving CIFAR10 (ID) vs SVHN (OOD) and Tiny-ImageNet (OOD). The results are from 15 runs and the best scores per uncertainty metric are in bold.

| Model | | $N$ | Method | EU Measure as Metric | | | | TU Measure as Metric | | | |
|---|---|---|---|---|---|---|---|---|---|---|---|
| | | | | SVHN (OOD) | | Tiny-ImageNet (OOD) | | SVHN (OOD) | | Tiny-ImageNet (OOD) | |
| | | | | AUROC | AUPRC | AUROC | AUPRC | AUROC | AUPRC | AUROC | AUPRC |
| VGG16 | BNNR | 10 | Baseline | 86.60±1.28 | 90.54±1.00 | 85.00±0.27 | 80.90±0.42 | 88.63±1.49 | 93.26±1.10 | 85.77±0.27 | 82.93±0.35 |
| | | | Ours | **88.38±1.53** | **92.61±1.12** | **86.28±0.25** | **83.88±0.32** | **88.99±1.61** | **93.45±1.17** | **86.44±0.27** | **84.28±0.34** |
| | | 50 | Baseline | 86.60±1.37 | 90.44±1.02 | 85.41±0.21 | 81.79±0.30 | 88.67±1.54 | **93.29±1.12** | 86.02±0.24 | 83.31±0.30 |
| | | | Ours | **88.90±1.65** | **92.75±1.22** | **87.17±0.26** | **85.22±0.33** | **89.17±1.69** | 93.24±1.25 | **87.22±0.26** | **85.35±0.33** |
| | BNNF | 10 | Baseline | 86.67±0.54 | 90.64±0.71 | 84.78±0.18 | 80.51±0.38 | 88.31±0.50 | 93.05±0.50 | 85.44±0.19 | 82.53±0.34 |
| | | | Ours | **88.03±0.52** | **92.55±0.52** | **85.79±0.18** | **83.29±0.28** | **88.58±0.53** | **93.31±0.51** | **85.99±0.19** | **83.80±0.29** |
| | | 50 | Baseline | 86.63±0.60 | 90.56±0.79 | 85.10±0.19 | 81.28±0.34 | 88.34±0.53 | 93.07±0.51 | 85.63±0.20 | 82.80±0.32 |
| | | | Ours | **88.60±0.56** | **92.91±0.54** | **86.61±0.21** | **84.64±0.27** | **88.86±0.55** | **93.34±0.54** | **86.67±0.21** | **84.82±0.27** |
| ResNet-18 | BNNR | 10 | Baseline | 88.46±1.23 | 93.19±0.77 | 85.85±0.22 | 81.58±0.37 | 88.24±1.29 | 92.71±0.85 | 86.43±0.24 | 83.22±0.40 |
| | | | Ours | **88.61±1.26** | **93.35±0.83** | **86.16±0.20** | **82.99±0.26** | **88.53±1.29** | **93.09±0.88** | **86.63±0.21** | **83.91±0.35** |
| | | 50 | Baseline | 88.43±1.27 | 93.33±0.77 | 85.58±0.23 | 81.70±0.42 | 88.28±1.27 | 92.74±0.84 | 86.45±0.24 | 83.25±0.40 |
| | | | Ours | **88.93±1.24** | **93.61±0.83** | **86.48±0.21** | **83.80±0.34** | **88.84±1.26** | **93.35±0.86** | **86.82±0.22** | **84.38±0.36** |
| | BNNF | 10 | Baseline | 88.77±0.85 | 93.45±0.56 | 85.97±0.31 | 81.83±0.27 | 88.49±0.83 | 92.93±0.50 | 86.48±0.34 | 83.26±0.35 |
| | | | Ours | **88.96±0.83** | **93.62±0.55** | **86.28±0.33** | **83.22±0.36** | **88.84±0.81** | **93.36±0.52** | **86.70±0.33** | **84.03±0.35** |
| | | 50 | Baseline | 88.79±0.95 | 93.59±0.61 | 85.67±0.35 | 81.88±0.35 | 88.54±0.82 | 92.97±0.50 | 86.49±0.33 | 83.30±0.35 |
| | | | Ours | **89.30±0.83** | **93.89±0.55** | **86.59±0.33** | **83.99±0.35** | **89.18±0.81** | **93.64±0.54** | **86.90±0.32** | **84.53±0.36** |

in the case of 3 classes, if there are three distinct extreme probability vectors (three vertices of the simplex), our credal wrapper method will effectively convey complete uncertainty, with the resulting credal set encompassing the entire simplex. This conservative nature can be sensible, as it expresses our full ignorance of the correct classification.

Furthermore, we conduct an additional ablation study to explore the benefit of our method given overconfident prediction samples. We manually and randomly transform one of the predictions of the same input image from five deep ensembles to a one-hot probability and compare the OOD detection performance of our method and the classical approach. Table 13 also shows our credal wrapper can improve the uncertainty quantification even in overconfident scenarios.

Table 13: OOD detection using EU (left) and TU (right) as uncertainty metrics in overconfident scenarios. The results are from 15 runs, based on the ResNet-50 backbone. The best scores per uncertainty metric are in bold.

| Model | Method | Epistemic Uncertainty Measure as Metric | | | | Total Uncertainty Measure as Metric | | | |
|---|---|---|---|---|---|---|---|---|---|
| | | SVHN (OOD) | | Tiny-ImageNet (OOD) | | SVHN (OOD) | | Tiny-ImageNet (OOD) | |
| | | AUROC | AUPRC | AUROC | AUPRC | AUROC | AUPRC | AUROC | AUPRC |
| DE | Baseline | 90.42±0.81 | 93.30±0.86 | 87.01±0.20 | 83.53±0.28 | 94.36±0.45 | 96.98±0.32 | 88.54±0.19 | 86.82±0.30 |
| | Ours | **94.92±0.39** | **97.26±0.25** | **88.98±0.17** | **87.42±0.27** | **95.24±0.38** | **97.48±0.23** | **89.12±0.17** | **87.74±0.27** |

### A.4 Qualitative Evaluation of Uncertainty Estimation of Credal Wrapper

In this section, we present the estimates of the EU and TU on the ID and OOD samples of the classical DE (using $H(\tilde{\boldsymbol{p}}) - \tilde{H}(\boldsymbol{p})$ and $H(\tilde{\boldsymbol{p}})$, respectively) and our credal wrapper (using $\overline{H}(\mathbb{P}) - \underline{H}(\mathbb{P})$ and $\overline{H}(\mathbb{P})$, respectively) in Figures 9 and 10. The results qualitatively demonstrate that our credal wrapper consistently enhances the uncertainty quantification of classical DEs. This is evidenced by the significantly larger uncertainty estimates for the OOD samples, which correspond to the expected and desirable behavior.

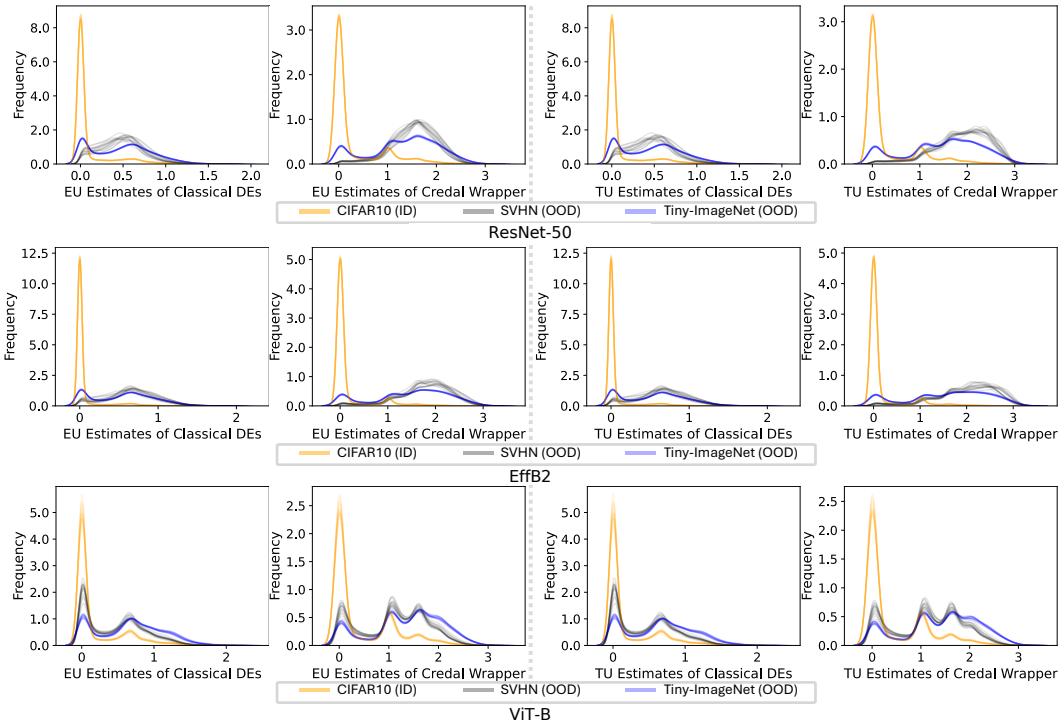


Figure 9: EU and TU estimates of ID (CIFAR10) and OOD (SVHN and Tiny-ImageNet) samples of the classical and credal wrapper version of DEs, obtained using ResNet-50, EffB2, and ViT backbones. Results are from 15 runs.

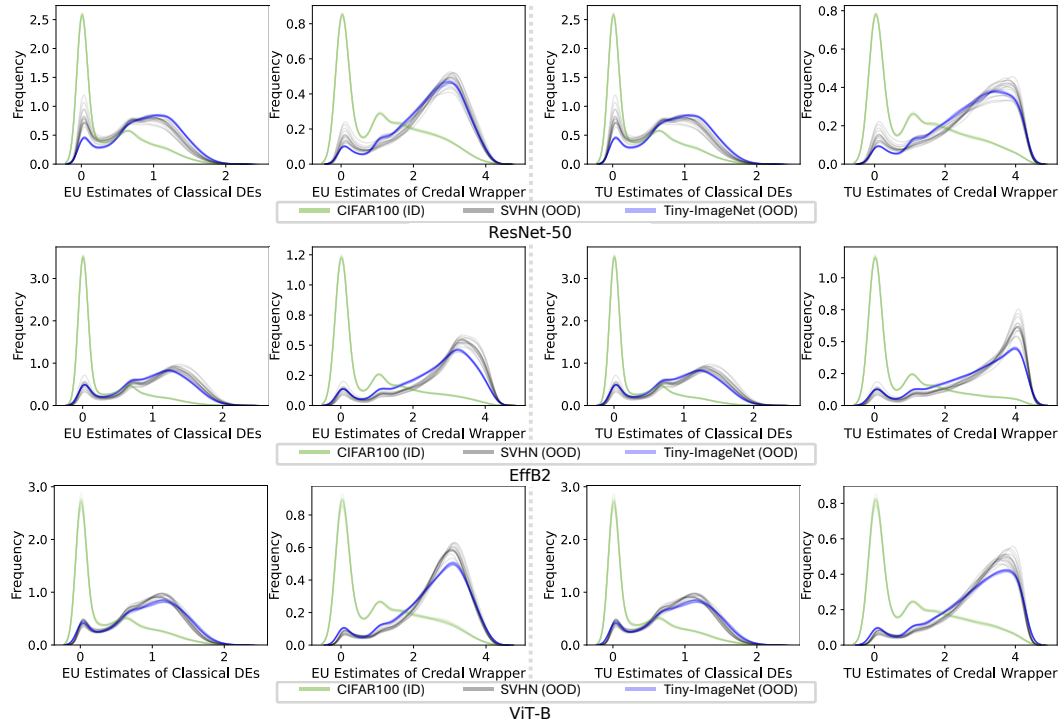


Figure 10: EU and TU estimates of ID (CIFAR100) and OOD (SVHN and Tiny-ImageNet) samples of the classical and credal wrapper version of DEs, obtained using ResNet-50, EffB2, and ViT backbones. Results are from 15 runs.

### A.5 Evaluation of Intersection Probability on Corrupted Samples using NLL Metric

In this section, we further evaluate the intersection probability on corrupted samples using the negative log-likelihood (NLL) metric. A smaller NLL indicates that the model is more confident and accurate in predicting the correct class for each input (Dusenberry et al., 2020). Figures 11 and 12 show the consistent superiority of the intersection probability on corrupted data in extensive test cases, as evidenced by smaller NLL values.

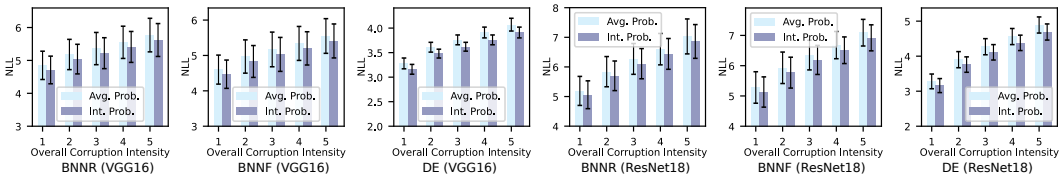


Figure 11: NLL values of BNNR, BNNF, and DE on CIFAR10-C against increased corruption intensity, using the averaged probability (Avg. Prob.) and our proposed intersection probability (Int. Prob.). VGG16 and ResNet-18 are backbones. Results are from 15 runs.

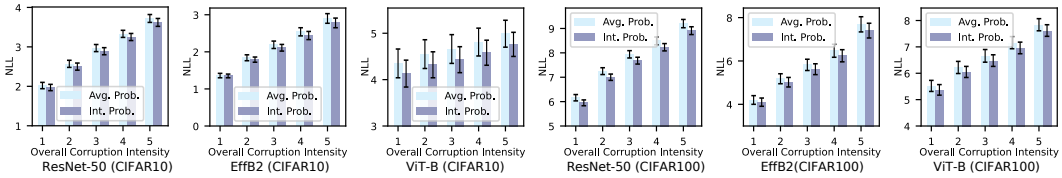


Figure 12: NLL values of DEs on CIFAR10-C and CIFAR100-C against increased corruption intensity, using the averaged probability (Avg. Prob.) and our proposed intersection probability (Int. Prob.). ResNet-50, EffB2, and ViT-B are backbones. Results are from 15 runs.

### A.6 Ablation Study on Hyperparameter of PIA Algorithm

In this experiment, we investigate the effect of the hyperparameter $J$ of the PIA algorithm 1. The OOD detection tasks include CIFAR100 (ID) vs SVHN (OOD) and Tiny-ImageNet (OOD) and deep ensembles are implemented on the ResNet-50 backbone. Table 14 shows OOD detection performance and the time cost for uncertainty quantification per sample, using different settings of $J$ for the PIA algorithm. The evaluation indicates that the proposed PIA algorithm can significantly reduce the computational complexity of estimating uncertainty in cases of high-class classification while maintaining superior uncertainty performance on OOD detection benchmarks. We can also observe that increasing the value of $J$ improves the OOD detection performance, but can lead to an increase in execution time. This is because solving the constrained optimization problem in eq. (8) involves more variables and constraints.

**Computational Cost** The reported time in Table 14 cost is measured on a single Intel Xeon Gold 8358 CPU@2.6 GHz, without optimization in the calculation process. As a reference, the time cost of the classical method for uncertainty quantification per sample is $0.007_{\pm 0.001}$ms. In addition, the time cost for CIFAR10 without reduction can also be seen as 7.18ms from Table 14. While high, it remains practical without limiting computational resources. We also believe a more efficient code implementation of our approach could significantly mitigate the computational cost.

## B Experimental Implementation Details

**Training Details** In terms of the evaluation using the small-scale datasets, all models are implemented on the established VGG16 and ResNet-18 architectures using the CIFAR10 dataset. The Adam optimizer is applied with a learning rate scheduler, initialized at 0.001, and subjected to a 0.1 reduction at epochs 80 and 120. Standard neural networks (SNNs) and BNNs are trained for 100 and 150 epochs, respectively. Standard data augmentation is uniformly implemented across all methodologies to enhance the training performance quality of training data and training performance. The

Table 14: OOD detection AUROC and AUPRC performance (%) of credal wrapper of DEs using EU (left) and TU (right) as uncertainty metrics, and the time cost, using different setting of $J$ of PIA algorithm. The OOD detection involves CIFAR100 (ID) vs SVHN (OOD) and Tiny-ImageNet (OOD). The results are from 15 runs, based on the ResNet-50 backbone.

| $J$ | EU as Metric | | | | TU as Metric | | | | Time Cost per Sample (ms) |
|---|---|---|---|---|---|---|---|---|---|
| | SVHN | | Tiny-ImageNet | | SVHN | | Tiny-ImageNet | | |
| | AUROC | AUPRC | AUROC | AUPRC | AUROC | AUPRC | AUROC | AUPRC | |
| 10 | 78.81±1.87 | 87.96±1.09 | 80.17±0.19 | 75.25±0.26 | 80.05±1.92 | 89.30±0.97 | 81.24±0.14 | 77.60±0.18 | 7.182±0.087 |
| 20 | 80.22±1.96 | 89.40±1.03 | 81.00±0.16 | 77.16±0.23 | 80.71±1.96 | 89.97±0.99 | 81.46±0.14 | 78.29±0.17 | 11.346±0.038 |
| 100 | 80.55±1.99 | 89.68±1.04 | 81.16±0.16 | 77.76±0.21 | 80.90±1.98 | 90.07±1.00 | 81.52±0.14 | 78.50±0.15 | 109.469±1.330 |

training batch size is set as 128. The device is a single Tesla P100-SXM2-16GB GPU. The standard data split is applied. In terms of EDDs, for each learning rate scheduler configuration, as discussed in Section 4, we train 15 models for 100 epochs, one from each distinct DE. All other training configurations, such as data splitting and augmentation, are kept consistent with those used for the other models. Additionally, temperature annealing, outlined in the original EDD paper (Malinin et al., 2019), is also applied during the EDD training process.

In terms of the evaluation using the large-scale datasets, we mainly use two Tesla P100-SXM2-16GB GPUs as devices to contract deep ensembles by independently training 15 standard neural networks (SNNs) under different random seeds. The input shape of the networks is (224, 224, 3). The Adam optimizer is employed, with a learning rate scheduler set at 0.001 and reduced to 0.0001 during the final 5 training epochs. Concerning the CIFAR10 dataset, SNNs are trained using 15, 15, and 25 epochs for ResNet-50, EffB2, and ViT-B backbones, respectively. As for the CIFAR100 dataset, SNNs are trained using 20, 20, and 25 epochs for ResNet-50, EffB2, and ViT-B backbones, respectively. Note that models based on ViT-B backbones are trained on one single Nvidia A100-SXM4-40GB GPU. In the ImageNet experiments, we employ one single Nvidia A100-SXM4-40GB GPU to retrain SNNs based on a pre-trained ResNet-50 model for 3 epochs, using the Adam optimizer with an initialized learning rate of $1e^{-6}$, under different random seeds. Standard data split is applied to all training processes. In ImageNet experiments, we apply three epochs as we observed that increasing the number of epochs further leads to lower validation loss and accuracy. The choice of not training them from scratch is mainly due to computational constraints. Although this setting may have implications for the performance of ensembles, regardless of the absolute baseline performance of ensembles under different training settings, our method exhibits a consistent improvement.

The experiment codes are provided in the supplementary files.

Table 15: Poor ID prediction and OOD detection performance of EDD-Fair. CIFAR10 as ID data.

| Model | | ID Prediction Performance | | OOD Detection Performance using EU | | | |
|---|---|---|---|---|---|---|---|
| | | | | SVHN (OOD) | | Tiny-ImageNet (OOD) | |
| | | ACC (%) | ECE | AUROC | AUPRC | AUROC | AUPRC |
| VGG16 | EDD-fair | 56.57±12.56 | 0.249±0.047 | 56.60±12.35 | 71.10±7.51 | 55.73±4.75 | 51.32±3.19 |
| ResNet-18 | EDD-fair | 85.68±3.48 | 0.102±0.056 | 85.30±7.85 | 90.16±5.95 | 76.84±4.59 | 69.84±4.29 |

**OOD Detection Process** In this paper, the OOD detection process is treated as a binary classification. We label ID and OOD samples as 0 and 1, respectively. The model's uncertainty estimation (using the EU or TU) for each sample is the 'prediction' for the detection. In terms of performance indicators, the applied AUROC quantifies the rates of true and false positives. The AUPRC evaluates precision and recall trade-offs, providing valuable insights into the model's effectiveness across different confidence levels.

**ECE Evaluation Process** In the context of ECE, a 'well-calibrated' prediction is expected to have a confidence value of 80% and be correct in approximately 80% of the test cases. To calculate ECE, predictions are split into a predetermined number $Q$ of bins $B$ of equal confidence range. The ECE is then calculated by summing the absolute difference between the average accuracy and confidence

within each bin (Mehrtens et al., 2023):

$$\text{ECE} := \sum_{g=1}^{G} \frac{|B_g|}{n} \Big| \text{acc}(B_g) - \text{conf}(B_g) \Big|, \tag{16}$$

where $|B_g|$ is the number of samples in the $g$-th bin and $n$ is the total number of samples.

## C Discussion on Generating Credal Sets from Individual Probability Distributions

Given a finite set of probability predictions, a possible alternative method for generating a credal set, termed *convex hull* approach, also exists. This method involves directly constructing the convex hull from the finite set of predictions. In our *credal wrapper*, the probability intervals define the credal set by injecting upper and lower bounds per class in eq. (5) and eq. (6), whereas the *convex hull* method requires computing all vertices of the credal sets.

The theoretical underpinning for the convex hull method when reasoning with coherent lower probabilities (and, therefore, the corresponding credal sets) is that it allows us to comply with the coherence principle (Walley, 1991). In a Bayesian context, individual predictions (such as those of networks with specified weights) can be interpreted as subjective pieces of evidence about a fact (e.g., what is the true class of an input observation). Coherence ensures that one realizes the full implications of such partial assessments (Walley, 1991; Cuzzolin, 2008). Figure 13 conceptually shows the differences between two methods in a 2D simplex.

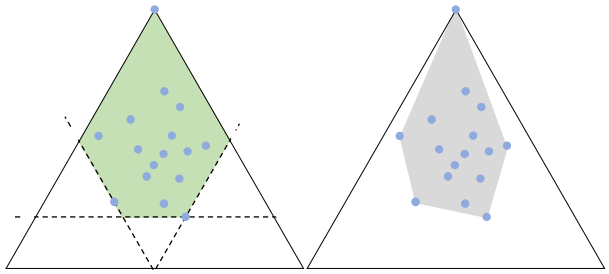

Figure 13: Different credal set generation methods. Left: our *credal wrapper*; right: *convex hull*.

Compared to the *convex hull* method, our probability interval systems exhibit a more conservative nature. Another practical difference is that the *convex hull* method is highly computationally complex, preventing it from being practically implemented in multi-class classification tasks. In the following, we aim to explain the associated complexity of the calculation process.

Given such a coherent lower probability, denoted as $\underline{P}$, the associated credal set $\mathbb{K}(\underline{P})$ comprises all probability measures ($\mathcal{P}(\mathbb{Y})$) in the target space ($\mathbb{Y}$) that can be defined as follows:

$$\mathbb{K}(\underline{P}) := \{P \in \mathcal{P}(\mathbb{Y}) \mid P(\mathbb{A}) \geq \underline{P}(\mathbb{A}) \; \forall \mathbb{A} \subseteq \mathbb{Y}\}. \tag{17}$$

Further, $\underline{P}$ is considered coherent if it can be computed as:

$$\underline{P}(\mathbb{A}) = \min_{P \in \mathbb{K}(\underline{P})} P(\mathbb{A}) \; \forall \mathbb{A} \subseteq \mathbb{Y} \tag{18}$$

where $\mathbb{A}$ denotes any possible subset of the target space $\mathbb{Y}$.

Mapping the finite set probabilistic predictions to a credal set generally requires the following steps:

i) Compute the lower probability for any subset $\mathbb{A}$ of the target space $\underline{P}(\mathbb{A})$.

ii) Compute the masses over the subsets by using Möbius inverse (Chateauneuf & Jaffray, 1989):

$$m_{\underline{P}}(\mathbb{A}) = \sum_{\mathbb{B} \subseteq \mathbb{A}} (-1)^{|\mathbb{A} \setminus \mathbb{B}|} \underline{P}(\mathbb{B}) \quad \forall \mathbb{A} \subseteq \mathbb{Y}. \tag{19}$$

iii) Compute the vertices of the credal set $\mathbb{K}(\underline{P})$. Its vertices are all the distributions $P^\pi$ induced by a permutation $\pi = \{x_{\pi(1)}, \dots, x_{\pi(|\mathbb{Y}|)}\}$ of the elements of its sample space $\mathbb{Y}$, of the form (Chateauneuf & Jaffray, 1989; Cuzzolin, 2008)

$$P^\pi[\underline{P}](x_{\pi(i)}) = \sum_{\mathbb{A} \ni x_{\pi(i)};\ \mathbb{A} \not\ni x_{\pi(j)}\ \forall j<i} m_{\underline{P}}(\mathbb{A}) \tag{20}$$

The vertex (the extreme probability) assigns to each class, put in position $\pi(i)$ by the permutation $\pi$, the mass of all the focal elements (sets of classes with non-zero mass) containing it, but not containing any elements preceding it in the permutation order (Wallner, 2005).

The above procedure is quite computationally expensive, because i) When the number of classes $|\mathbb{Y}| = C$ is large, it can be highly inefficient to compute probabilities for all $2^C$ events in the power set of $\mathbb{Y}$). ii) Compute the vertices in eq. (20) is extremely computationally difficult.

On the contrary, the probability interval systems applied do not suffer such computational burden, as shown in eq. (5) and eq. (6), the resulting credal set is directly defined by $C$ pairs probability bounds over classes. The extensive experimental validation also strongly demonstrates the consistently improved uncertainty performance of our proposed *credal wrapper*.

# D Discussion on Credal Wrapper in Cases of Infinite Samples

In this section, we aim to discuss the behaviour of the credal wrapper and the associated intersection probability in the case of infinitely many samples from individual probability distributions. In this context, we assume that the support of the sampled distribution spans the entire simplex, without imposing any additional distributional constraints.

If we assume the predictions are sampled from a 'second-order' distribution (as in the BNN case), when one keeps collecting samples the corresponding credal set in eq. (6) expands (as it relies on min/max probability calculations in eq. (5)). Therefore, as $\boldsymbol{p}^*$ is a function of the *probability interval bounds* of the credal set (and not the actually collected samples), for $N$ that goes to infinity will tend to the $\boldsymbol{p}^*$ of the probability simplex $\Delta$, i.e., the uniform distribution. Indeed, this does not happen to the BMA theoretically, which averages the samples. However:

(i) The argument for the rationality of the representative $\boldsymbol{p}^*$ of an interval probability system is compelling (Cuzzolin, 2009; 2022). The same asymptotic effect is shared by the center of mass of the credal set, indicating that this is a feature inherent to the credal representation itself.

(ii) In practice, $N$ is small even in the general cases of BNNs ($N = 5$). In the ablation study in Section 4, we examine the performance of our credal wrapper in cases of $N = 10$, $N = 50$, and even $N = 1000$, our credal wrapper consistently shows an improved uncertainty estimation and calibration performance, as shown in Tables 5, 6 and Figures 3, 11. As the practical performance of $\boldsymbol{p}^*$ is better than BMA, it appears that BMA can be biased/less representative at $N$ never going to infinite w.r.t. $\boldsymbol{p}^*$, whereas it enjoys better convergence properties.

(iii) This does not apply to ensembles, as ensemble members are not 'sampled' from any distribution. The ablation study in Section 4 as well as Figures 3, 5, 11, 12 suggest that the consistent superior performance of $\boldsymbol{p}^*$ of calibration performance on corrupted data.

# E Result visualizations

## E.1 Visualization of credal set predictions and intersection probability

Visualizing credal sets in high-dimensional ($C$) classification tasks is challenging, as it requires a $(C-1)$-dimensional probability simplex. To demonstrate our credal wrapper method, we consider a three-class classification scenario derived from the CIFAR10 classification tasks in the main body, focusing on the classes 'airplane', 'automobile', and 'others'. The class 'others' includes the remaining class indices in the original CIFAR10 datasets. We visualize our credal wrapper of ResNet50-based DEs and VGG16-based BNNRs using different sample sizes on the 2D simplex in Figures R1 and R2. Three cases are considered: the correctly classified in-distribution (ID) sample (left), the incorrectly classified sample (middle), and the OOD samples (right).

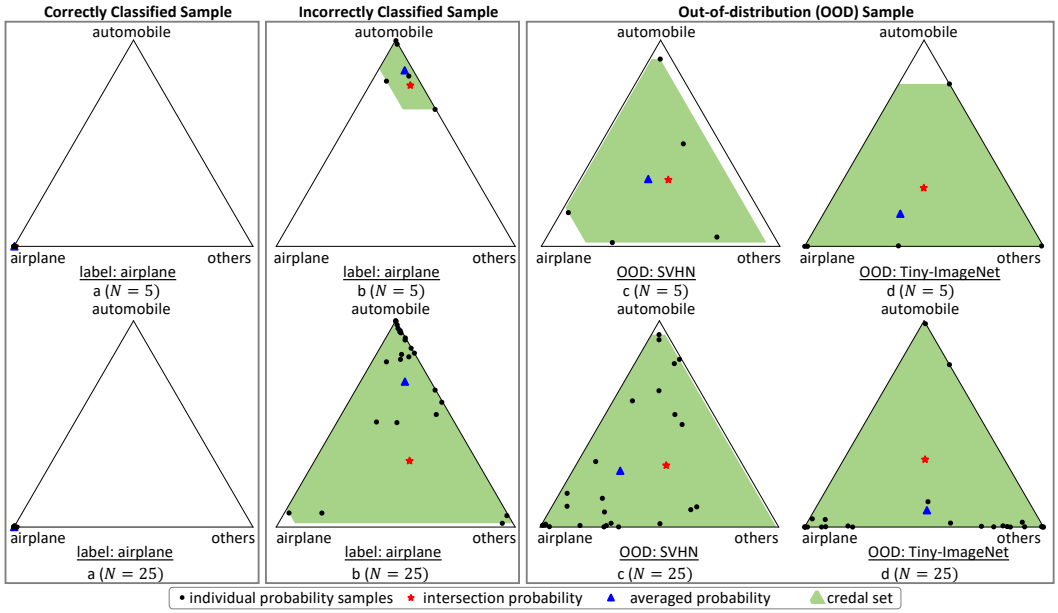


Figure R1: Visualization of our credal wrapper of ResNet50-based DEs on different ensemble sizes ($N = 5$ and $N = 25$) in three cases: correctly classified in-distribution (ID) sample (left), incorrectly classified sample (middle), and OOD samples (right).

From the visualizations, we observe that the differences between individual predictive probability samples for correctly classified ID data and the resulting discrepancy between the intersection probability and the averaged probability are less visible. However, for incorrectly classified samples, the differences become more apparent. Since the intersection probability is derived from probability intervals, it tends to exhibit less overconfidence in incorrect predictions. A similar observation can be seen in Figure R3, where the individual probabilities, the corresponding intersection probability, and the averaged probability for the CIFAR10 and CIFAR10-C (corrupted) samples are visualized. Furthermore, as the ensemble size increases, this reduction in overconfidence becomes even more apparent (Figures R1 and R2). These observations explain the comparable performance of the intersection probability and the averaged probability in terms of test accuracy and expected calibration error (ECE) on ID data but improved performance on corrupted data.

Figures R1 and R2 also illustrate that the credal sets for incorrectly classified and OOD samples are notably larger than those for correctly classified ID samples. This behavior aligns with the construction of our credal wrapper, which is formulated by extracting the upper and lower probability limits per class from individual probability samples. It also shows that the credal sets naturally expand when newly sampled probabilities fall outside the original bounds (for example, the OOD cases in Figures R1 and R2), reflecting a conservation property that reasonably incorporates new evidence rather than disregarding it. This phenomenon can also explain why the OOD detection performance can be further enhanced with an increased sample size, as observed in Tables 4 and 6 in the main body. Furthermore, the theoretical foundation for uncertainty quantification using credal sets and probability interval systems is robust, as detailed in Appendix §A.1 and Appendix §D.

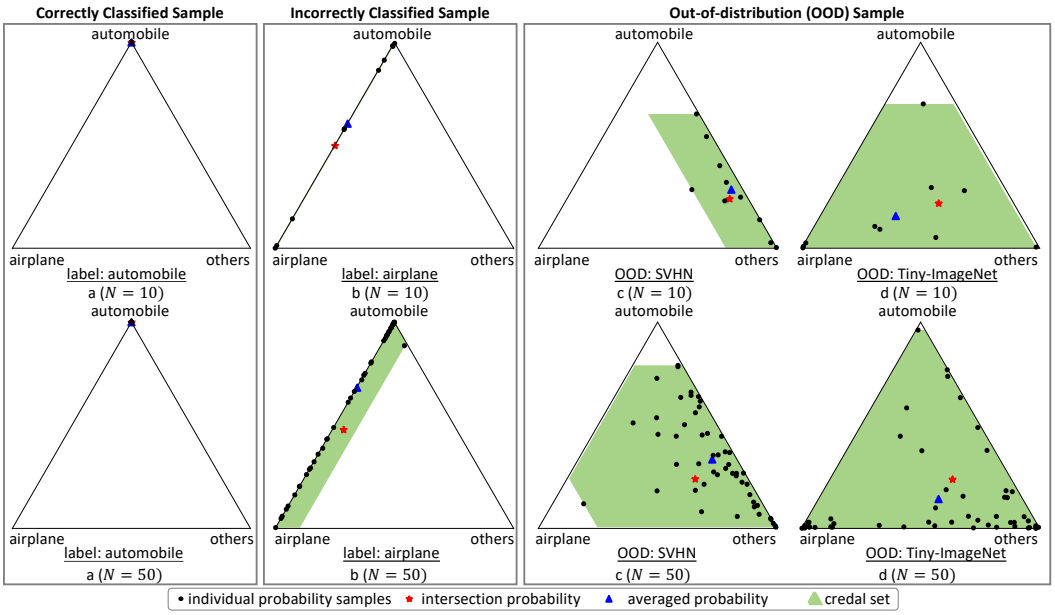


Figure R2: Visualization of our credal wrapper of VGG16-based BNNRs on different sample sizes ($N = 10$ and $N = 50$) in three cases: correctly classified in-distribution (ID) sample (left), incorrectly classified sample (middle), and OOD samples (right).

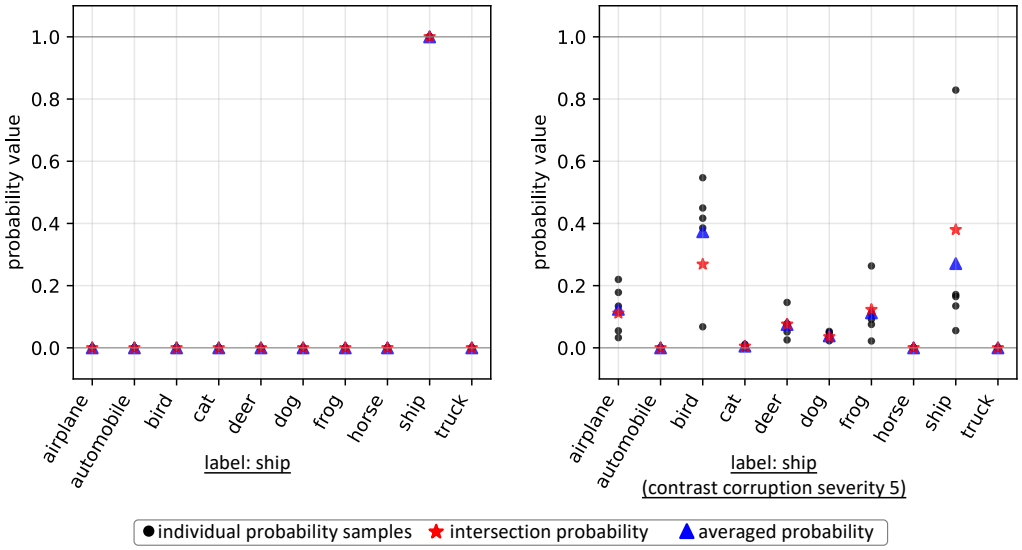


Figure R3: Visualization of the individual probabilities, the intersection, and the averaged probability for one CIFAR10 sample and its corrupted version sample. For the corrupted data, the intersection probability can remain the correct prediction while the averaged probability leads to wrong prediction.

### E.2 Visualization of uncertainty estimates using different hyperparameters of PIA Algorithm

The hyperparameter $J$ of the PIA algorithm 1 is a design choice intended to mitigate the computational cost associated with uncertainty quantification, particularly in situations with limited computational resources. As demonstrated in the ablation study results in Table 14, the proposed PIA algorithm significantly reduces the computational complexity of uncertainty estimation in high-class

classification scenarios, while maintaining strong uncertainty performance on OOD detection benchmarks. Increasing the value of $J$ enhances the performance. Furthermore, we present the EU and TU estimates for both ID (CIFAR100) and OOD (SVHN and Tiny-ImageNet) samples at different values of $J$ in Figure 4. The figure shows that using a small value of $J$ leads to an underestimation of the EU and TU, particularly for OOD samples. This phenomenon explains why a higher value of $J$ can achieve better OOD detection performance.

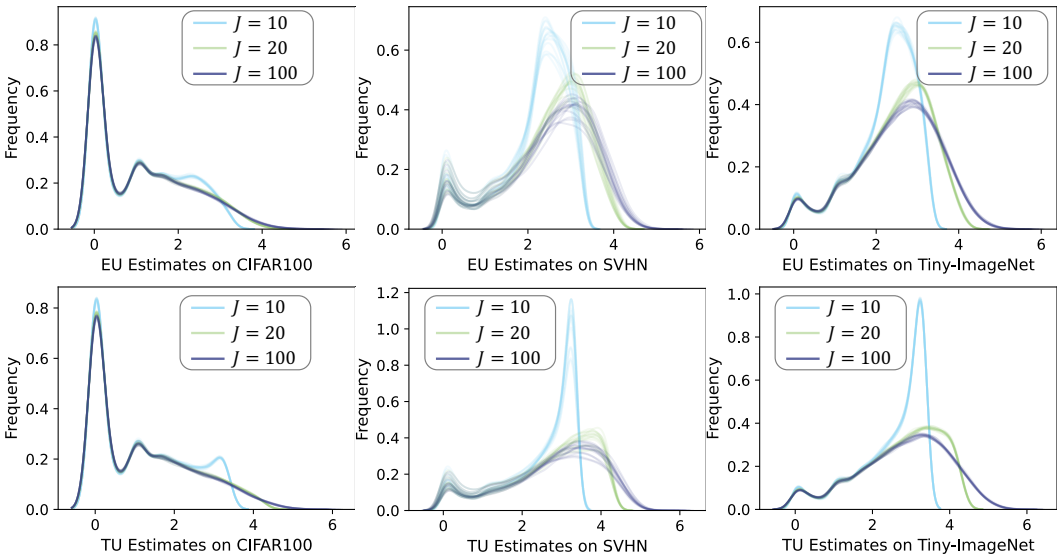


Figure R4: EU and TU estimates of ID (CIFAR100) and OOD (SVHN and Tiny-ImageNet) samples of the credal wrapper version of DEs using different values of $J$, obtained using the ResNet-50 backbone. Results are from 15 runs.